Journal of Structural Geology, Vol. 15, Nos 3–5, pp. 609 to 628, 1993
Printed in Great Britain

0191-8141/93 $06.00+0.00

Deformation resulting from regional extension during pluton ascent and emplacement, central Sierra Nevada, California

OTHMAR T. TOBISCH

Department of Earth Sciences, University of California, Santa Cruz, CA 95064, U.S.A.

PAUL R. RENNE

Geochronology Center, Institute of Human Origins, 2453 Ridge Road, Berkeley, CA 94709, U.S.A.

and

JASON B. SALEEBY

Division of Geological and Planetary Sciences, California Institute of Technology, Pasadena, CA 91125, U.S.A.

(*Received* 20 *December* 1991; *accepted in revised form* 27 *August* 1992)

Abstract—Solid-state foliation, lineation, small-scale folds and domainal shear zones have developed in pre-existing granitic and minor metasedimentary wallrock during a combined deformation involving a regional extensional strain and ascent and emplacement of the Mt Givens pluton (MGP). Mylonite is common throughout much of the ~1–2 km wide, 10 km long shear zone, with ultramylonite best developed near the contact with the MGP, which itself lacks significant solid-state deformation. Migmatization accompanies ultramylonite formation in the northern half of the zone, but both these features are poorly developed or absent in its southern half where the shear zone is distributed over a wider area. Strain estimates across the shear zone using microgranitic enclaves as markers show a positive gradient and an increasing ratio of simple shear/pure shear towards the MGP.

Microprobe analyses on hornblende and plagioclase yield pressure and temperature estimates of ~3.5 kb and ~680°C respectively, during shear zone formation, at least at its late stages of development. Zircon Pb/U and $^{40}Ar/^{39}Ar$ ages constrain timing of the high-temperature movement on the shear zone to ~90 Ma, essentially the age of the MGP, although movement immediately prior to that time appears likely. We speculate that a regional extensional shear zone was developing prior to the emplacement of the MGP, which, as it ascended, heated the wallrock facilitating both further strain in the zone as well as buoyant rise of the pluton along the zone. The MGP was near its critical melt fraction during the last several kilometers (?) of its ascent, and could have possessed sufficient viscosity (strength) to impose a weak shear strain on the shear zone rocks, although most of the foliation and extensional features in the zone are probably related to the regional strain field. Late-stage folding of the foliation is attributed to shouldering aside of the wallrock by the MGP during the last increment of its ascent and final emplacement.

INTRODUCTION

General

CRETACEOUS plutons of the central Sierra Nevada batholith are known to become generally younger eastward (Stern *et al.* 1981, Chen & Moore 1982), and the compiled data of Bateman (1988) document the widespread occurrence of magmatic foliation in these plutons. Discrete domains of solid-state deformation also occur, and recent work is showing that the solid-state deformation has formed within four different dynamic and/or kinematic frameworks: that related to: (a) dynamics of pluton ascent and emplacement; (b) dextral strike-slip shear zones (transpression); (c) regional extension; and (d) regional contraction, with the last three associated with some stage of pluton emplacement and/or cooling.

We are currently studying several domains of solid state deformation which affect both granitoids and their contiguous wallrocks in the central Sierra Nevada (Fig. 1.) and further to the south. The domains dip moderately to steeply, are of variable length (10–40 km or greater), and commonly are related to regional tectonic activity showing either dip-slip (Tobisch *et al.* 1990, McNulty 1991, Tong 1991) or strike-slip movement (Busby-Spera & Saleeby 1990, Gazis and Saleeby 1991, Tikoff & Teyssier 1991, Saleeby 1992). Other regions of solid-state deformation in the central Sierra Nevada appear related to pluton emplacement dynamics (e.g. Bateman *et al.* 1983) or show a polygenetic origin (this study).

The Courtright shear zone was originally mapped by Bateman (1965) and co-workers (Bateman *et al.* 1984). They concluded that the shear zone most likely resulted from a regional tectonic event which predated emplacement of the Mount Givens pluton (MGP), and was time correlative with shear zones mapped to the northwest by Peck (1980). Below we delineate the geometry and development of solid-state fabric, give strain estimates associated with foliation development, and consider its thermobarometric and geochronological (Pb/U, $^{40}Ar/^{39}Ar$) aspects. We interpret the Courtright shear zone as

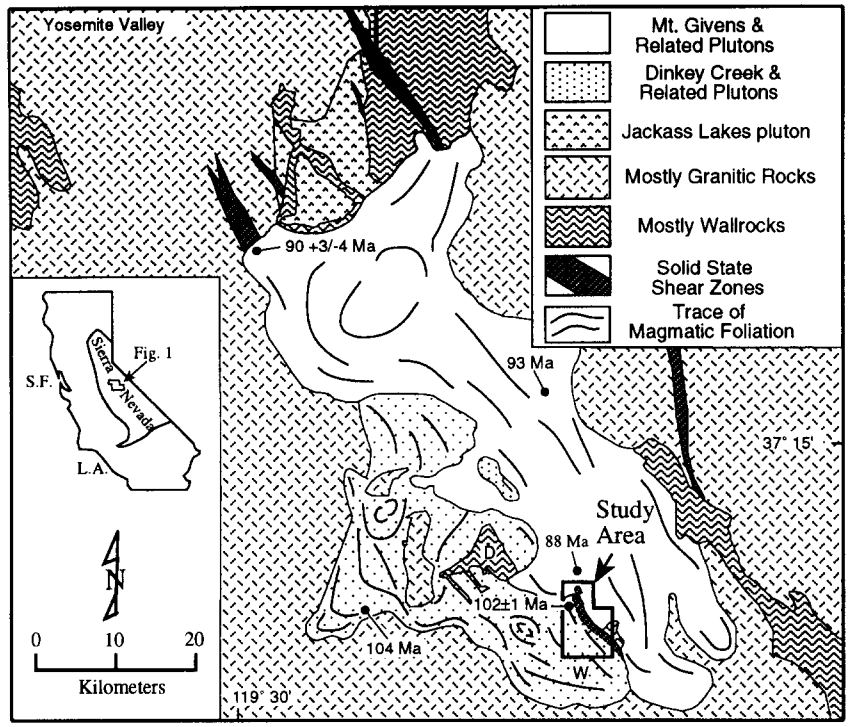

Fig. 1. Simplified geologic map of part of the central Sierra Nevada, showing specific features of the Mt Givens and Dinkey Creek plutons (for clarity, other related but smaller plutons discussed in the text are not shown on the map) and their relation to the study area. Zircon Pb/U ages showing error (±) are from this study, others are from Stern *et al.* (1981). W = Wishon Reservoir, D = Dinkey Creek pendant. Map modified from Bateman (1988); shear zone northeast of study area modified from Lockwood & Lydon (1976) and B. Tikoff (personal communication, 1991).

the combined result of a regional extensional strain field and the dynamics of ascent and emplacement of the MGP.

Rock types, ages and magmatic structures

The Courtright zone is an ~0.8–2 km wide and ~10 km long steeply dipping zone of ductile strain developed within the border of three plutons of the Shaver Intrusive Suite (Bateman 1988) and adjacent wallrock screens where they lie against the undeformed MGP (Fig. 1). At its northern extremity, the shear zone is cut off by the undeformed Eagle Peak granodiorite; at its southeastern extremity, the shear zone disappears under glacial deposits overlying the MGP (Bateman 1965). The wall rocks, mostly impure sandstone and calc-silicate rock with minor semipelite, occur as uncommon screens and blocks, and probably are correlative with sedimentary rocks in the Dinkey Creek pendant ~10 km to the west (locality D in Fig. 1). These multideformed pendant rocks lack fossils, and based on lithologic correlation may be of Paleozoic or Mesozoic age (Kistler & Bateman 1966, Merritt 1985, Lahren & Schweickert 1989).

In the study area, the Shaver Intrusive Suite consists of three intrusives: (a) the Dinkey Creek pluton (DCP), which is a mafic hornblende–biotite granodiorite that contains abundant microgranitic enclaves (Fig. 2, closely spaced dots); (b) the granite of Short Hair Creek, a somewhat more felsic biotite–hornblende granodiorite with substantially fewer enclaves (Fig. 2, widely spaced dots); and (c) the relatively small granite of Lost Peak, a biotite leucogranite mostly devoid of enclaves (cf. Bateman 1965, 1988, Bateman & Wones 1972). The contact between the granite of Short Hair Creek and DCP was not observed and its exact locality in Fig. 2 is uncertain.

Zircon from a sample of DCP on the border of the shear zone (Fig. 2) yielded a concordant Pb/U age of 102 ± 1 Ma (see Geochronology section for details). Magmatic foliation is well-developed in many plutons of the batholith (Fig. 1) (Bateman 1965, 1988, Bateman & Wones 1972, Lockwood & Bateman 1976). In the study area, it is weakly to moderately developed within the three plutons, and is defined (Paterson *et al.* 1989) by aligned clots of biotite and/or hornblende, individual mafic grains, plagioclase and microgranitic enclaves. Magmatic lineation is weakly developed, and in general has been much less commonly mapped (e.g. Bateman & Wones 1972), perhaps in part because of the difficulty of identifying and accurately measuring it in rounded granitic exposures.

The Mount Givens pluton (MGP) ranges in composition from tonalite to granite (Bateman & Nokleberg 1978). It is the largest single pluton in the central Sierra Nevada batholith (Bateman 1988), with *minimum* dimensions of ~15 × ~80 km. Throughout much of the tonalitic to granodioritic parts, magmatic foliation is weakly to moderately well developed, but in the more differentiated (quartz monzonitic to granitic) parts, foliation is weak or absent (e.g. Bateman 1965, Bateman *et al.* 1971). In the study area, it is a hornblende–biotite granodiorite with relatively few microgranitic enclaves and a weakly to moderately developed magmatic foliation which becomes very weak ~100 m from the contact. Various other magmatic structures such as unusual (fish-

net) schlieren, strongly developed mafic layering and trains of enclaves occur in the border facies of the MGP at Courtright (Bateman *et al.* 1984). Zircon from a sample in the far northwest corner of the pluton (Fig. 1.) gave a discordant Pb/U age of $90^{+3/-4}$ Ma (see Geochronology section for details).

The Eagle Peak pluton (EP, Fig. 2.) is a hornblende–biotite granodiorite with a more felsic granite core, and it has been observed to intrude the MGP (Bateman & Wones 1972, Bateman & Nokleberg 1978); however, ages in the EP (K/Ar) and MGP ($^{40}Ar/^{39}Ar$ and Pb/U) suggest the two plutons are largely contemporaneous (cf. Stern *et al.* 1981, Noyes *et al.* 1983, and this study).

SOLID-STATE STRUCTURES

Geometry and orientation

Wallrocks. According to Kistler & Bateman (1966) and Merritt (1985), wallrocks in nearby areas to the northwest (Fig. 1, D) were multiply deformed prior to emplacement of the granitic rocks. In the study area, however, solid-state structural elements such as foliation and stretching lineation found within granitoids in the shear zone show a similar intensity of development and orientation as those structures in wallrock screens, suggesting that some component of wallrock strain may be emplacement-related.

Further, the larger wallrock screen in area C (Fig. 2) shows an intensely developed stretching lineation (Fig. 3a.) and mylonitic fabric is also well developed locally. This septum has been intruded by felsic dikes (~2 m maximum width) of the MGP, and both dike and earlier-formed mylonitic foliation–lineation strongly folded (Fig. 4a). Microscopic fabric of the dikes shows variations between essentially undeformed to weakly deformed, suggesting the dikes were in a 'mush' stage when they were emplaced and folded. These observations indicate that at least the later folds–crenulations in this wallrock screen are contemporaneous with the MGP, and may be related to pluton emplacement dynamics.

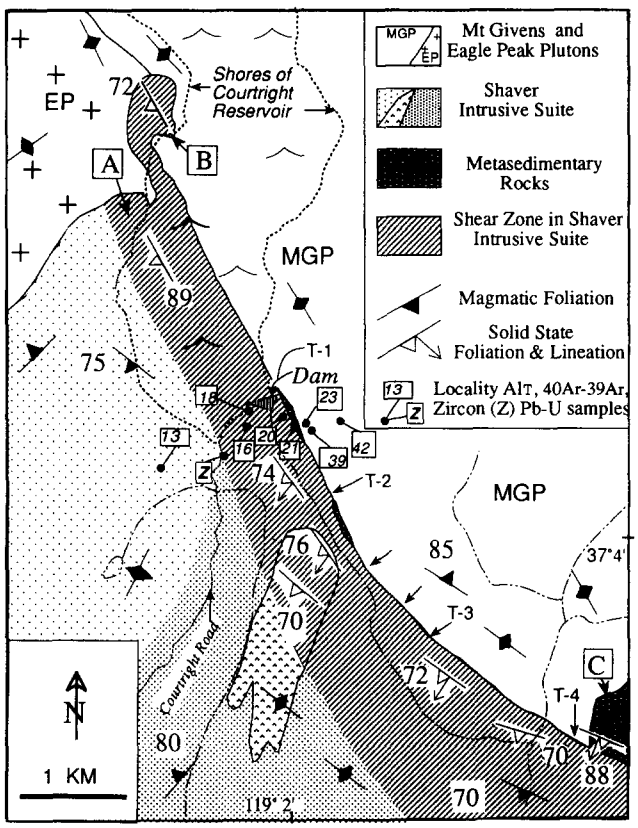

Fig. 2. Geologic map of the area showing the relation between the ductile shear zone, the Mt Givens (MGP) and Eagle Peak (EP) plutons, intrusives of the Shaver Intrusive Suite, and isolated screens of wallrock (dimensions of screens slightly exaggerated for clarity of pattern). Plutons of the Shaver Intrusive Suite are the Short Hair Creek (widely-spaced dots), the Dinkey Creek (DCP, closely-spaced dots) and the Long Peak (inverted v-dots). The shear zone has not been shown in the wallrock to preserve clarity. Exact placement of contacts within the Courtright reservoir are uncertain. Map modified from Bateman (1965) and Bateman & Wones (1972). Letters A-C, T-1, T-2, etc., and unadorned arrows between T-2 and T-3 are localities discussed in the text.

Mt Givens Pluton (MGP). With the exceptions of weak to moderate subgrain formation in quartz and relatively rare kinking of plagioclase twins, the main body of the MGP in the Courtright area is free from solid-state deformation. Along parts of its border on the west side of Courtright Reservoir (locality A, Fig. 2.), however, solid-state deformation is locally developed within an apparent coeval magma that has mingled with Mt Givens magma during its ascent–emplacement. The coeval magma occurs as accumulations of mafic enclaves in a host somewhat more mafic than the MGP, which itself has been invaded by the Mt Givens and Eagle Peak granodiorites. The stretched enclaves lie in a foliation developed from magmatic and lesser solid-state processes, and has subsequently been folded (Fig. 4b). Key exposures show the deformed enclave-rich magma cutting the solid-state foliation in the DCP. From these observations, it seems reasonable that the enclave-rich magma intruded the shear zone at a late stage of movement immediately prior to the emplacement of the MGP.

Structures developed in granitoids within the shear zone

Foliation, lineation and folding of the foliation occur within the DCP, Short Hair Creek and Long Peak granitoids in the shear zone (Fig. 2). In the field, the most prominent and widespread structure is foliation, which generally is a combination of magmatic and solid-state strain (S_1), and in outcrop is seen mostly as aligned individual and clots of mafic minerals (Fig. 4c). Lineation occurs as elongate clots of biotite–hornblende, aligned hornblende and long axes of microgranitic enclaves (Fig. 3b). Orientation of structures in the granitoids and the wallrock shows a 'normal' scatter with a mean foliation of ~150°/80°SW; the mean stretching lineation is oriented 212°/77°, with a pitch of ~80° in the foliation (Fig. 6a).

Domainal kinking, folding and crenulation of the

foliation also occurs. On a basis of geometry and orientation, these structures can be divided into extensional and contractional sets. The extensional set ($S_{2\,ext}$) occurs as discrete zones of shearing and displacement of S_1 and microgranitic enclaves, in which the west side is displaced down (Figs. 3c and 4c); these structures appear essentially contemporaneous with S_1. In a few thin-sections sampled close to the MGP, weakly developed E-directed (west-side-up) microshears (*S–C* fabric) were observed, and are probably related to $S_{2\,ext}$ as discussed later. Melt segregations are found lying parallel to $S_{2\,ext}$ locally. The contractional set ($S_{2\,con}$) varies from very tight folding of mylonite and/or ultramylonite (Figs. 4a & d) to more open to tight folding of microgranitic enclaves in the precursor phase of the MGP (Fig. 4b) and in the wallrock. Melt segregations (quartzo-feldspathic layers) have also been observed lying parallel to the axial plane of the more open ($S_{2\,con}$) folding (Fig. 4b), suggesting high temperature prevailed during S_2. The orientation of axial planes of the domainal late structures is generally northwest with steep dips (Fig. 6b), whereas axes are moderately to steeply plunging (and very difficult to measure). $S_{2\,ext}$ shows a tendency towards steeper dips and more constant strike than $S_{2\,con}$. In addition, minor domains of kinking, crenulation and narrow ultramylonite zones showing highly variable orientation occur close to the contact with the MGP. Field observations suggest these and most of the $S_{2\,con}$ structures are probably related to emplacement dynamics of the MGP.

Microstructural development in the shear zone

Solid-state strain in the shear zone is heterogeneous both within a given exposure and regionally along strike. In general, the development of ultramylonite increases substantially towards the MGP, with its maximum development in area B in the northwest (Fig. 2.) where it may be tens of meters wide and is accompanied by especially well-developed migmatization. Southeast of the dam, migmatization becomes rare or absent, and the shear zone crops out as a wider, more diffuse zone. West of area C (Fig. 2.) the western part of the zone is characterized largely by incipient recrystallization (intercrystalline strain) of the magmatic fabric.

A traverse across the zone at Courtright dam (T-1, Fig. 2.) shows the progressive development from magmatic structures through mylonite to ultramylonite textures (Figs. 5a–c, respectively). On the edge of the zone, foliation in thin-section is defined by clots of biotite–hornblende and alignment of longitudinally twinned plagioclase, features typical of a magmatic structure (Paterson *et al.* 1989). Solid-state effects are uncommon but include kinking of large biotite grains, weak subgrain development in quartz and bent plagioclase twins, all of which may be the result of late-stage emplacement movement. Recrystallization fabrics of quartz, biotite and hornblende showing some preferred orientation are the first unambiguous evidence of shear zone deformation, and these, with plagioclase and K-feldspar, form new smaller grains (Figs. 5b & c). However, the recrystallization and deformation tend to be domainal, and igneous and metamorphic phases of the same mineral may coexist in a given thin-section.

Quartz morphology can be weakly to moderately elongate (Fig. 5b) and shows deformation bands locally, indicative of crystal-plastic mechanisms; however, it more commonly forms equidimensional grains with near 120° boundaries (Fig. 5c). Further within the zone, domains of strongly elongate quartz can be found locally in some thin-sections. Closer to the contact with the MGP, ultramylonite zones develop, and are characterized by essentially complete recrystallization of the igneous assemblage (Fig. 5c). Quartz typically has recrystallized to equi-dimensional grains in these rocks, although rarely relict igneous quartz in a few thin sections of ultramylonite preserve dimensional ratios as high as 12:1. Visual evaluation of weak quartz deformation band orientation (using a quartz wedge to determine fast–slow vibration directions) suggests ⟨*a*⟩ slip is predominant, although relic deformation bands in many grains support the interpretation that high temperature ⟨*c*⟩ slip was active at some stage in the deformation. In one sample of ultramylonite taken from a few meters from the MGP contact (sample TC-21, Fig. 2), large porphyroblasts of clinopyroxene occur and overprint a strongly aligned biotite fabric; we consider the clinopyroxene as a contact metamorphic effect that post-dates the mylonitization.

Microstructural changes along other traverses are comparable but vary in intensity. For example, west of area C (Fig. 2), ultramylonites and complete recrystallization of the primary fabric are less common, and igneous plagioclase and hornblende tend to be more persistent even near the contact with the MGP, with the western border of the shear zone expressed as incipient recrystallization of myrmekite colonies and plagioclase rims.

STRAIN AND KINEMATICS OF THE SHEAR ZONE

Strain estimates from shape of microgranitic enclaves

Various workers have used the shapes of microgranitic enclaves (henceforth referred to as *enclaves*) to estimate the strain in granitic rocks (e.g. Ramsay 1975, 1989, Escorza 1978, Holder 1979, Courrioux 1987), and several techniques have been proposed to evaluate their original shape (e.g. Ramsay 1967, Hutton 1982, Ramsay & Huber 1983). Great care needs to be exercised in interpreting the strain from enclaves, however, since substantial change in enclave shape are known to occur over short distances as a result of magmatic flow in tectonically undeformed plutons (e.g. Vernon *et al.* 1988; our unpublished data). Once solid-state deformation has been superimposed onto a magmatically deformed enclave, it is very difficult to separate the effects of magmatic from solid-state strain.

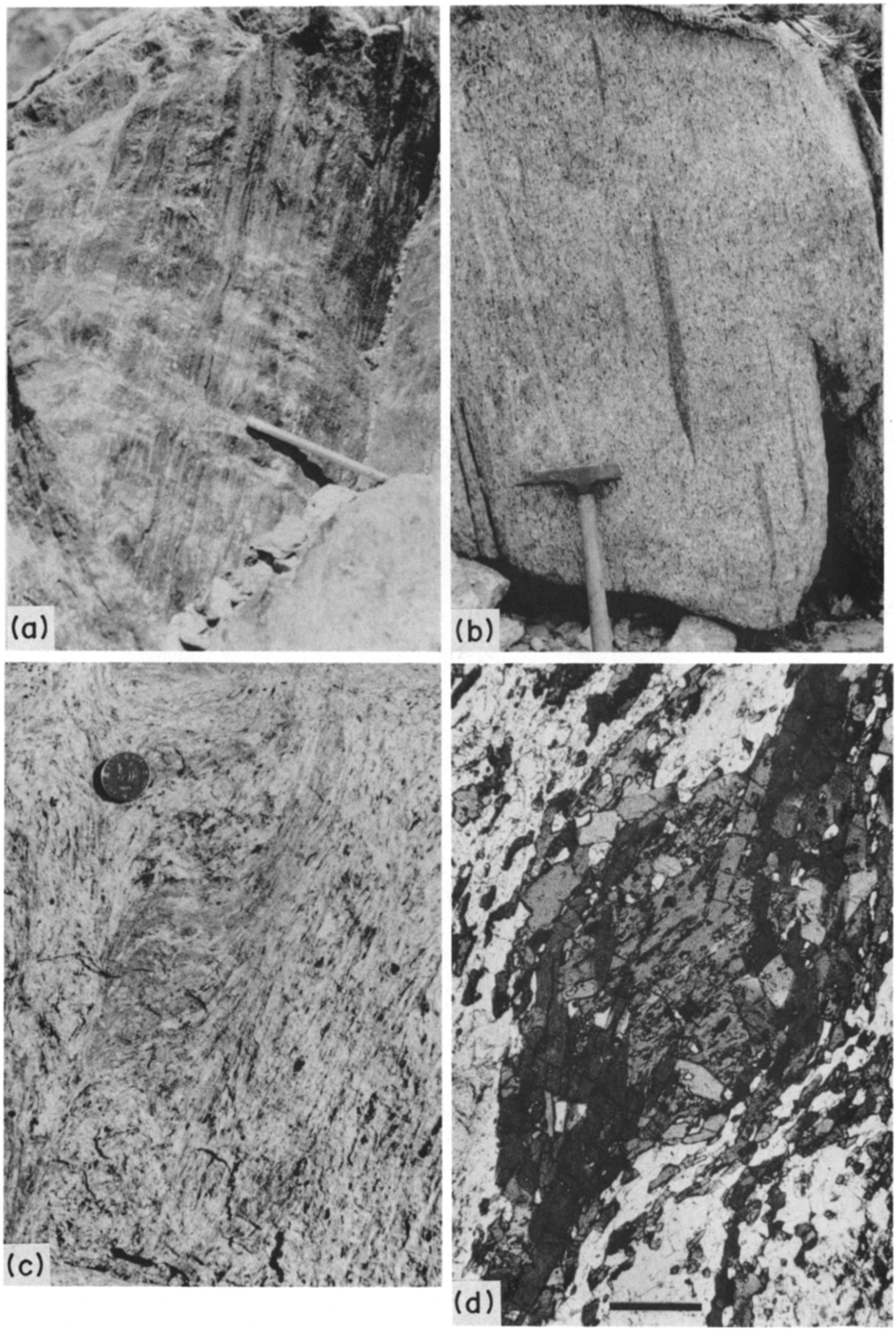

Fig. 3. Photographs of structural features. (a) Stretching lineation in wallrock lying in S_1, south of locality C, Fig. 2. The pencil is approximately 20 cm long. (b) Microgranitic enclaves in DCP showing composite fabric of mostly solid state with some relic magmatic strains. Locality is southeast of dam, Fig. 2, close to the contact with MGP. The hammer head is approximately 25 cm long. (c) Extensional $S_{2\,ext}$ structures showing west-side-(left) down; north of locality A, Fig. 2. The coin is approximately 3 cm in diameter. (d) Photomicrograph of an σ-type porphyroclast of igneous hornblende (core) and metamorphic hornblende tails; from the southern part of the shear zone near locality C, and showing west-side-(left) down. Bar scale is 0.4 mm.

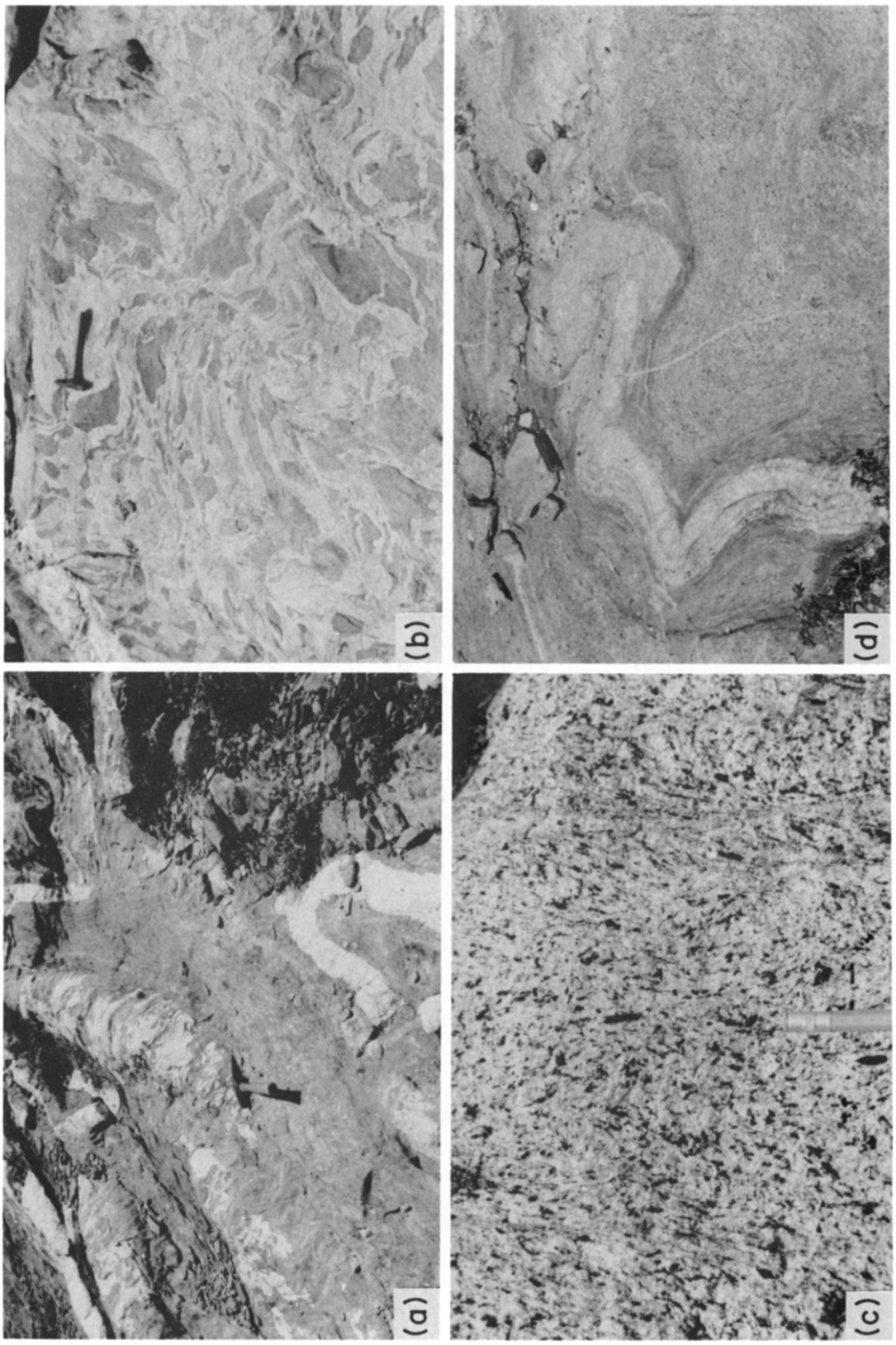

Fig. 4. Photographs of structural features. (a) S_{2con} folds with variably plunging axes folding dikes–sills of MGP which have intruded largely parallel to the mylonitic foliation (S_1), near locality C, Fig. 2. The fold axis at the hammer is essentially horizontal and folds the stretching lineation oriented normal to the fold axis. The hammer head is approximately 25 cm long. (b) S_{2con} folds folding enclaves stretched during magmatic and solid-state deformation, and showing melt (quartzo-feldspathic) segregations lying parallel to their axial planes, locality A, Fig. 2. The hammer head is approximately 25 cm long. (c) S_1 foliation showing a composite of magmatic and solid-state components. Note aligned hornblende, clots of biotite + hornblende, and shear zones on the left- and right-hand sides of the photograph. The shear zone on the right shows a weakly developed *S–C* geometry indicating west-side-(left) down. Locality is near sample station 16, Fig. 2. The pencil is approximately 3 cm long. (d) S_{2con} folds in the DCP folding ultramylonitic foliation and quartz layers lying parallel to it; south of sample station 21, Fig. 2. The knife is approximately 10 cm long.

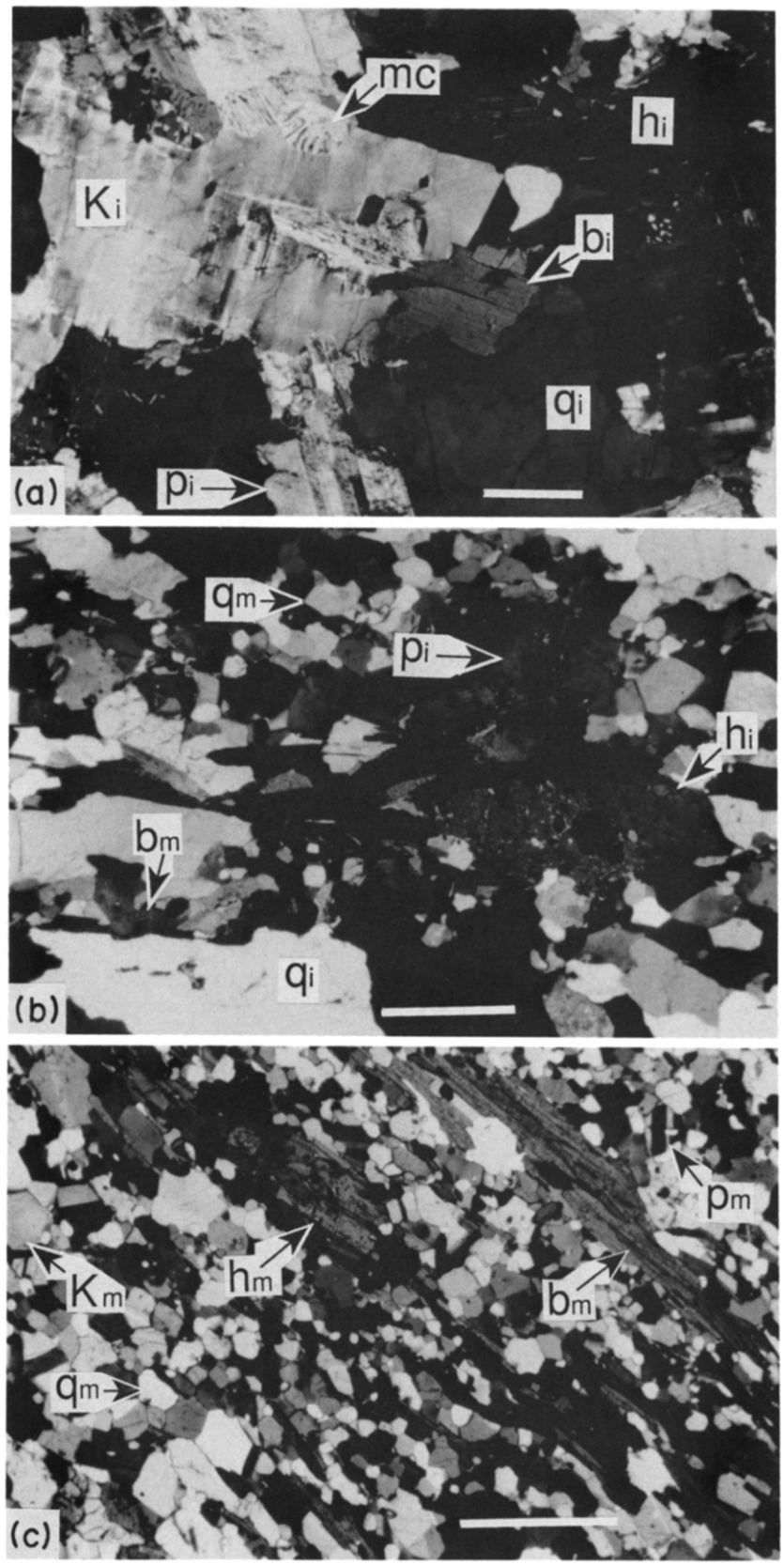

Fig. 5. Photomicrographs of foliation development in Shaver Lake Suite granitoids within the shear zone. For all figures, K_i = perthitic K-feldspar of igneous origin with patches of microcline; K_m = orthoclase of metamorphic origin; mc = myrmekite colonies; q_i = igneous quartz showing weak (in undeformed rocks) to moderate (in deformed rocks) subgrain formation; q_m = metamorphic quartz usually strain free, h_i and h_m = igneous and metamorphic hornblende, respectively; b_i and b_m = igneous and metamorphic biotite, respectively; and p_i and p_m = igneous and metamorphic plagioclase, respectively. Bar scale is 1 mm in all cases. (a) Primary igneous fabric in the Short Hair Creek granodiorite at station TC-13, Fig. 2. (b) Assemblage in Dinkey Creek granodiorite showing recrystallization and deformation at station TC-16, Fig. 2. Quartz shows some elongation. (c) Ultramylonite fabric developed in DCP ~10 m from the contact with MGP (station TC-21, Fig. 2), containing a completely recrystallized igneous assemblage, and with the addition of clinopyroxene (not shown); note that many quartzo-feldspathic grains are nearly equidimensional, and that S_1 is defined principally by alignment of metamorphic biotite and hornblende, with lesser enhancement by quartzo-feldspathic minerals.

In the Courtright area, we made measurements on enclave shape in parts of the DCP that had undergone magmatic-only strain and parts that had subsequently undergone solid-state strain. At each station showing magmatic-only strain, a *minimum* of 25 (R_f/ϕ) measurements (Ramsay & Huber 1983) were made on each of two surfaces approaching 90° to each other, highly inclined to the foliation, and one surface of which was picked to include the stretching lineation wherever it was observable. [Axes of the strain ellipsoid are $X > Y > Z$, where changes in length (+ or − elongations) are $X = \varepsilon_1$, $Y = \varepsilon_2$ and $Z = \varepsilon_3$. Strain magnitude is $\varepsilon_s = 1/(3)^{1/2}[(\varepsilon_1 - \varepsilon_2)^2 + (\varepsilon_2 - \varepsilon_3)^2 + (\varepsilon_3 - \varepsilon_1)^2]^{1/2}$, and strain symmetry is $\nu = 2(\varepsilon_2 - \varepsilon_1 - \varepsilon_3)/(\varepsilon_1 - \varepsilon_3)$, where $\varepsilon = (1 + e)$, e = elongation $(l_1 - l_0)/l_0$, and where l_0 is the original and l_1 is the final length of any axis (Lode 1926, Nadai 1963).] In a 2–3 km strain traverse away from the shear zone (towards W, Fig. 1), the magnitude (ε_s) of magmatic strain was reasonably well-constrained over five stations (i.e. $\varepsilon_s \approx 0.50$–$0.80$), although strain symmetry (ν) was more variable (i.e. $\nu \approx -0.16$ to $+0.80$). We therefore think that the magnitudes of magmatic strain immediately outside the shear zone are a reasonable approximation to values within the zone prior to solid-state deformation.

At stations showing solid-state deformation, we did not usually measure the angle (ϕ) between enclave long-axis and foliation, because ϕ appeared to be very small (<5° at most stations), and it was very time consuming to measure angles accurately. We assessed the possible error of ignoring ϕ by considering that angle in two samples in which $1° < \phi < 5°$, and found the error in strain magnitude (ε_s) without measuring ϕ was negligible (<1%) at lower total strains ($\varepsilon_s \sim 0.6$), but was overestimated by approximately +10% where $\varepsilon_s \sim 2.0$.

Solid-state strain in the shear zone was estimated by calculating the total strain ellipsoid from enclave shape and subtracting an average value of ε_s and ν of magmatic strain measured immediately outside the shear zone. This operation used a matrix program which took into consideration ε_s, ν and the orientations of the initial (magmatic) and total (magmatic + solid state) strain ellipsoids. Two traverses across the entire zone (T-1 and T-2, Fig. 2) show a marked positive strain gradient towards the MGP (Fig. 7a). Two partial traverses (T-3 and T-4) within 200 m of the MGP also show increases in ε_s and a larger constrictional symmetry component towards the MGP as does T-1 (Fig. 7b). The remaining three stations shown in Fig. 7(b) all lie within ~150 m of the MGP contact between T-2 and T-3 (arrows lying along contact in Fig. 2), and show values comparable to the maximum shown in T-1 but with larger components of flattening.

Development of matrix foliation (Figs. 5a–c) along most traverses appears visually commensurate with the solid-state strains indicated (Figs. 7a & b). Locally, however, matrix foliation elements (e.g. weakly elongated primary(?) quartz or plagioclase poorly recrystallized) do not appear to sufficiently reflect the strain recorded by the enclaves. This inconsistency may indicate a local increase in magmatic strain intensity or a change in the pre-solid-state orientation of the magmatic foliation, which would affect the solid-state values calculated from the enclave data. Within the limitations discussed above, we regard the enclave shape data and the positive gradient towards the MGP as a conservative approximation to solid-state strain in the shear zone.

Kinematic plan

Kinematic indicators in the shear zone are not common. However, three lines of evidence at various scales suggest that displacement was down-dip in the shear zone (i.e. DCP (west-side) down). At the microscopic scale, σ-type clasts (Passchier & Simpson 1986) of igneous hornblende with recrystallized metamorphic hornblende tails have been observed lying in the foliation in a few specimens (Fig. 3d). As documented earlier, the stretching lineation shows an 80° pitch in the foliation (Fig. 6a). Within this geometric scheme, dis-

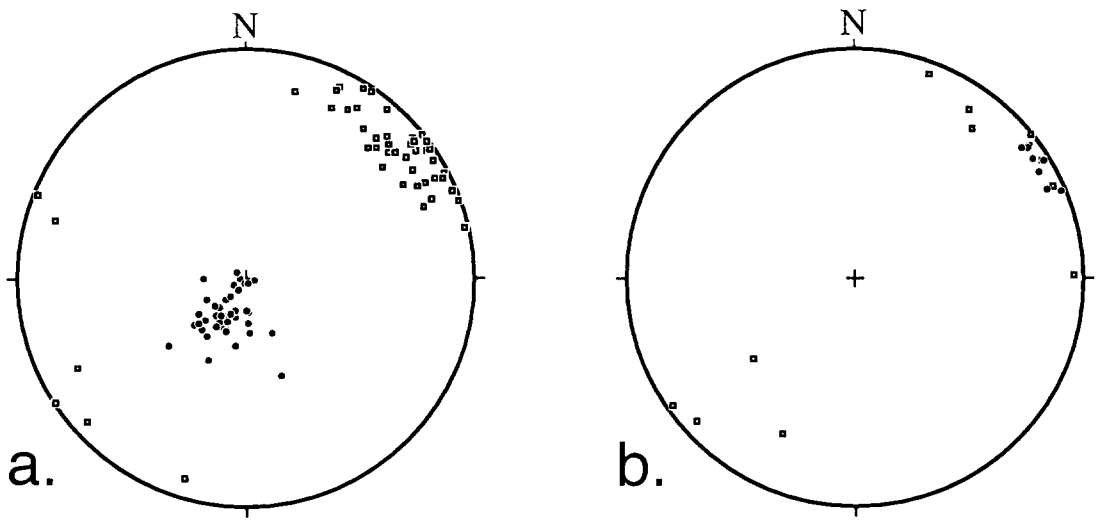

Fig. 6. Equal-area plots of structural elements in the study area. (a) Poles to S_1 foliation (open boxes) and stretching lineations (filled circles). (b) Poles to axial planes of S_{2con} (open squares) and poles to S_{2ext} (filled circles).

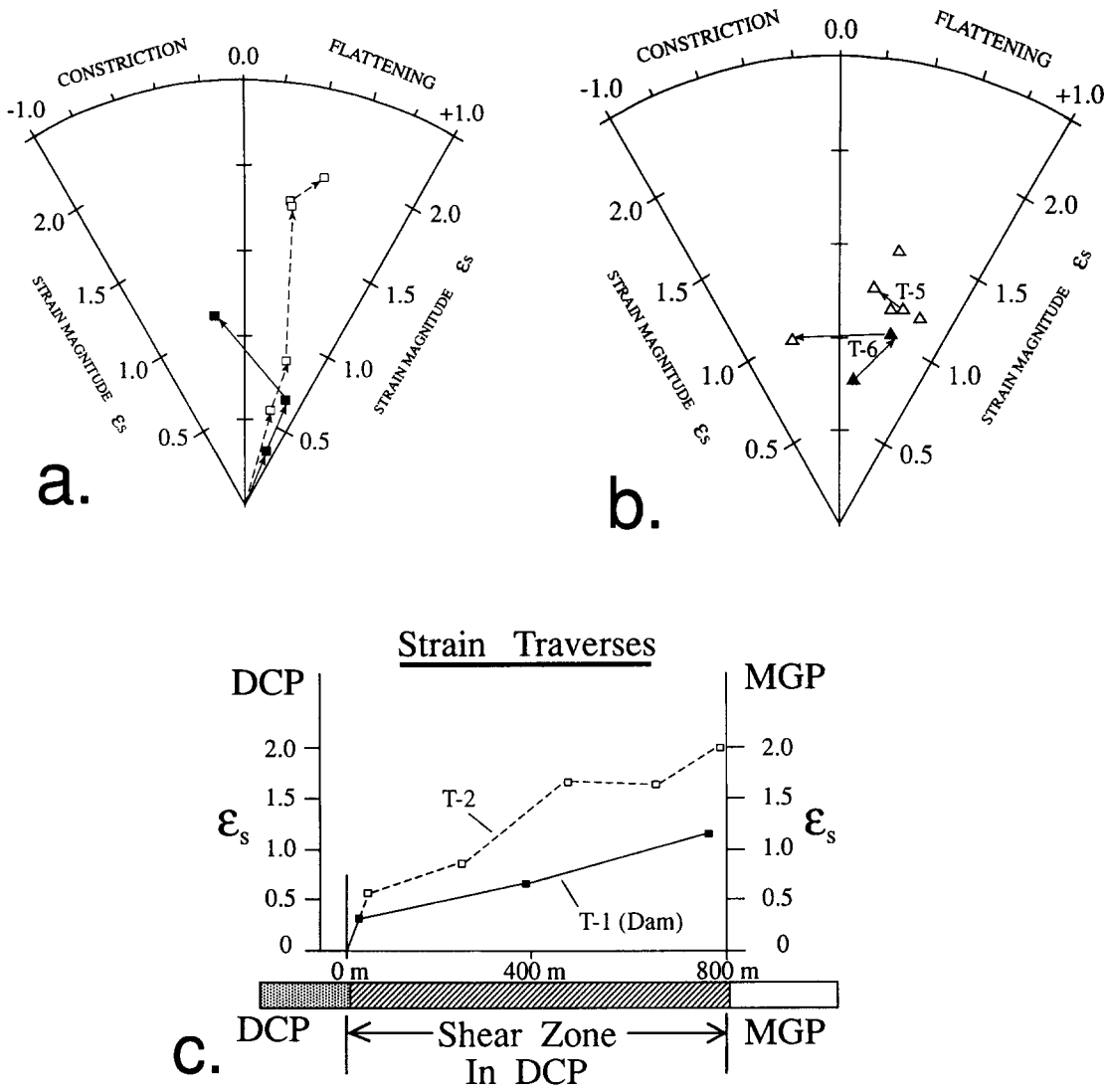

Fig. 7. (a) & (b) Hsu diagrams showing range of strain magnitude (ε_s) and symmetry (ν) in (a) traverses T-1 (filled symbols) and T-2 (open symbols) and (b) all other strain stations (open triangles = >25 measurements per face; filled triangles = five measurements per face). (c) Section across the shear zone along traverse T-1 (dam) and T-2 (Fig. 2) showing an increase in ε_s as the contact with the MGP is approached.

placement of synkinematic felsic dikes at outcrop scale indicate west-side-down movement. And lastly, as indicated earlier, shear sets associated with S_2 structures show two distinct orientations, $S_{2\,ext}$ defining a steeply dipping extensional set (Fig. 3c), and a more gently dipping reverse-sense shear zone set ($S_{2\,con}$) seen only in thin-sections close to the MGP. The two sets appear approximately conjugate relative to the main foliation (Fig. 8a). These geometric and kinematic relations are consistent with a very steeply W-dipping shear zone showing west-side-down movement (Fig. 8a), which is commensurate with the other kinematic indicators mentioned above. This geometry and kinematic plan implies the shear zone developed in an extensional environment; the amount of actual shear displacement along the zone is unknown.

Components of simple shear–pure shear in the zone

To estimate the components of pure and simple shear acting in the zone, we have plotted the strain data in Fig. 8(b) (modified after Coward & Kim 1981, Kligfield *et al.* 1981). The lower values of strain in the western half of the shear zone (see Fig. 7c, traverses T-1 and T-2) suggest the strain there has developed by a combination of simple (ss) and pure (ps) shear with $XZ_{ss}/XZ_{ps} \simeq 1$ (Fig. 8b). In the eastern half, however, that ratio increases as the contact with the MGP is approached. This is dramatically shown in T-2, where the ratio very near the contact with the MGP is $XZ_{ss}/XZ_{ps} \simeq 17$. In the partial traverses and isolated strain stations which fall in the eastern half of the shear zone, the increase is less dramatic but nevertheless apparent relative to other parts of the zone.

A review of the data shown in Figs. 3, 4, 6, 7(a)–(c) and 8(b) leads us to conclude that: (i) there is heterogeneous distribution of the two shear components in the zone but the simple shear component is most intense near the MGP (i.e. an average $\gamma \sim 3$ at 10 stations within ~200 m of the MGP); (ii) the shear component gradient was steep and diminished rapidly away from the MGP contact; and (iii) the presence of *symmetrical* $S_{2\,con}$ folds folding mylonitic foliation suggests that the MGP imposed a flattening strain on the wallrock during late stages of (diapiric) emplacement.

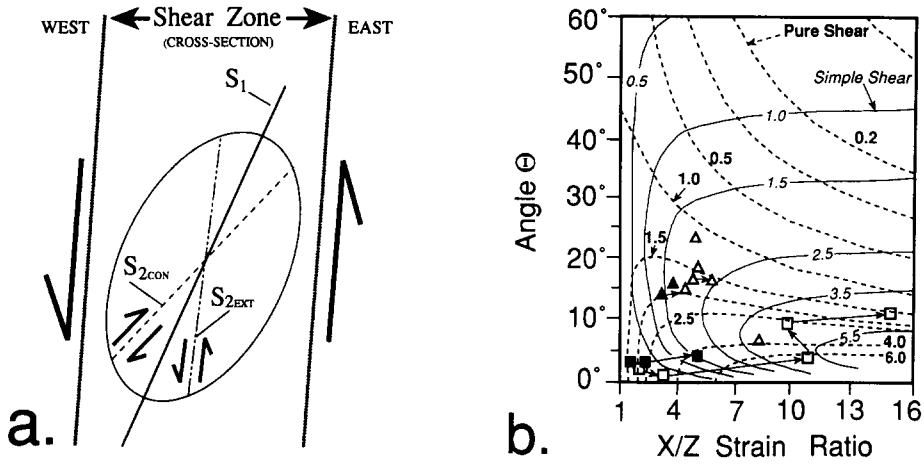

Fig. 8. (a) Diagram showing the relation of the main foliation and micro/mesoshears showing extensional and contractional geometries interpreted to indicate west-side-down movement along the main shear zone, which dips steeply to the west. (b) Plot illustrating components of pure shear and simple shear active in the deformation (modified from Coward & Kim 1981 and Kligfield *et al.* 1981). Θ is the angle between the shear zone boundary and the *X*-axis of the strain ellipsoid. Filled and open squares are as in Fig. 7(a), filled and open triangles as in Fig. 7(b); simple shear contours are a measure of the shear strain (γ). See text for details.

MINERAL ASSEMBLAGES AND THERMOBAROMETRY

Mineral assemblages in granitoids

All mineral assemblages in the granitoids contain quartz, plagioclase, K-feldspar, biotite, hornblende, titanite and iron ore (magnetite). Metamorphic changes across the shear zone generally do not produce an entirely new mineral assemblage; rather, the metamorphic equivalent of the same assemblage is the rule. Internal chemical–structural changes do take place in some mineral phases, and occur in three general (shear zone parallel) domains: (1) the western edge of the shear zone; (2) the greater bulk of the shear zone; and (3) ultramylonites in the eastern half, but predominantly near the boundary with the MGP. For example, K-feldspar occurs in various states related to these three domains as follows:

(1) igneous orthoclase with patches of perthite or microcline + abundant peripheral myrmekitic colonies (Fig. 5a) (cf. Vernon 1991);

(2) igneous orthoclase, perthite, metamorphic microcline, + rare myrmekite colonies;

(3) metamorphic orthoclase.

Mafic minerals change through the same three domains as follows:

(1) igneous hornblende and biotite (some late replacement of biotite by chlorite),

(2) igneous and metamorphic hornblende, metamorphic biotite (rare chlorite after biotite);

(3) metamorphic hornblende and biotite, and rarely, clinopyroxene (contact metamorphic overprint).

Microprobe analysis of plagioclase rims shows only slight change between domains (1) and (3) ($An_{30} \rightarrow An_{34}$). Changes in hornblende chemistry indicate a decrease in Al^{IV}, which is correlated with a decrease in alkali (Table 1) on the A site; there is no change in X_{Fe}, and negligible change in Ca/Na^{M4}.

The distribution of the mineralogical changes is very heterogeneous, however, and their development is in large part a function of strain intensity. Igneous and metamorphic assemblages often coexist in the same thin-section, even in small mylonitic domains immediately contiguous to the contact with the MGP where strain intensity has not produced ultramylonitic fabrics. Indeed, only in the ultramylonites is it clear that the igneous assemblage is entirely recrystallized.

Mineral assemblages in wallrock

Wallrocks show the following characteristic assemblages in quartzo-feldspathic, impure calcareous, and mafic rocks:

quartz–plagioclase ($An_{\sim 20}$)–biotite ± (titanite–epidote);
quartz–plagioclase–hornblende–biotite ± (K-feldspar);
quartz–diopside–hornblende ± (biotite–opaque);
quartz–K-feldspar–biotite ± (hornblende–plagioclase–epidote);
plagioclase–hornblende ± (quartz-epidote–titanite).

Chlorite occurs after biotite (and rarely hornblende) locally, which we consider a retrograde effect during cooling. In any event, the metamorphic assemblages in the granitic and metasedimentary rocks suggest temperature conditions in the shear zone were those corresponding to the transition between upper hornblende hornfels and pyroxene hornfels facies (Turner 1981).

Hornblende thermobarometry

We probed hornblende rims for total (Al^T) and plagioclase rims for An content in an attempt to estimate the physical conditions under which the shear zone developed and the plutons were emplaced. The DCP, Short Hair Creek and MGP all contain the critical mineral assemblage (q–pl–ksp–bi–hb–sph–mt + melt phase) for Al-in-hornblende barometry (Hammarstrom

& Zen 1986) and plagioclase–hornblende thermometry (Blundy & Holland 1990), as do the metamorphosed granitic shear zone assemblages. While the presence of a melt phase in the two shear zone assemblages (TC-18 and TC-21, Fig. 2.) is uncertain, the close proximity (10 m) to the MGP of at least TC-21 makes it likely that its temperature was close to the solidus during emplacement of the MGP. In any event, there is currently debate on whether the total alumina content (Al^T in hornblende) is predominantly pressure or temperature sensitive (Hammarstrom & Zen 1986, 1992, Hollister *et al.* 1987, Johnson & Rutherford 1989, Blundy & Holland 1990, 1992, Vyhnal *et al.* 1991, Poli & Schmidt 1992, Rutherford & Johnson 1992, Schmidt 1992), and we have interpreted the data cautiously.

Our microprobe data are given in Table 1 along with representative analyses, and estimates of pressure have been calculated using the experimentally determined equation P (±0.6 kb) = $-3.01 + 4.76Al^T$ of Schmidt (1992). In Table 2 we list Ague & Brimhall's (1988,

Table 1. Chemical composition of representative microprobe analyses of hornblende rims from four specimens. TC-13 is the undeformed Short Hair Creek granodiorite outside the shear zone; TC-18 (mylonite) and TC-21 (ultramylonite) are both DCP within the shear zone; TC-23 is undeformed MGP. Parentheses after values of average Al^T, Si^{IV} and anorthite content indicate the number of determinations made. Estimated errors for pressure values are approximately ±1 kb; i.e. ±0.6 kb from Schmidt (1991) and ±0.5 kb spread in our data between samples. Temperature was calculated from Blundy & Holland's (1990) equation using a mean pressure value (*P = 4.04 kb, †P = 3.47 kb) recalculated from the regional data listed in Table 2; the error in temperature estimates is ±75°C (Blundy & Holland 1990). The value in parentheses indicates the number of rim analyses per thin section

	Dinkey Creek Pluton (DCP)			Mt Givens (MGP)
Sample No.	TC-13	TC-18	TC-21	TC-23
SiO_2	43.96	45.61	46.17	46.15
TiO_2	0.83	0.73	1.02	1.13
Al_2O_3	8.37	6.99	6.90	7.09
FeO	18.42	17.96	17.88	14.36
MnO	0.68	0.76	0.49	0.49
MgO	9.80	10.28	9.50	12.49
CaO	11.11	11.33	11.19	11.46
Na_2O	1.31	1.11	0.86	1.35
K_2O	0.76	0.57	0.54	0.61
H_2O	1.88	1.91	1.89	1.92
F	0.13	0.09	0.06	0.13
Cl	0.04	0.04	0.15	0.06
Total	97.21	97.10	96.56	97.13
Si^{IV}	6.82	7.04	7.14	7.00
Al^{IV}	1.18	0.96	0.86	1.00
Al^{VI}	0.35	0.31	0.39	0.27
Total Al	1.53	1.21	1.25	1.27
Average Al^T	1.53 (8)	1.41 (10)	1.34 (3)	1.28 (6)
Average Si^{IV}	6.81 (8)	6.93 (9)	7.04 (3)	6.98 (6)
Plagioclase rim	An_{30} (4)	An_{31} (5)	An_{34} (3)	An_{31} (4)
Pressure	4.3 kb	—	—	3.1 kb
Temperature	710°C*	694°C†	678°C†	684°C†

Table 2. (Al^T) data from Ague & Brimhall (1988, appendix D, 200–400 series) recalculated using the equation $4.76Al^T - 3.01$ (Schmidt 1992), and from Table 1, this study (TC-series). Standard errors on average pressure values for Dinkey Creek, Mt Givens and Jackass Lakes plutons are ±0.14, ±0.13, and ±0.12, respectively. Procedures and assumptions for these samples (except TC-series) given in Ague & Brimhall (1988)

Dinkey Creek Pluton (102 ± 1 Ma)			Mt Givens Pluton ($90^{+3/-4}$ Ma)			Jackass Lakes Pluton (98 Ma)		
Sample No.	Al^T	Pressure (kb)	Sample No.	Al^T	Pressure (kb)	Sample No.	Al^T	Pressure (kb)
281	1.50	4.1	299	1.38	3.6	349	1.44	3.8
282	1.44	3.8	300	1.32	3.3	351	1.53	4.2
289	1.51	4.2	301	1.57	4.5	353	1.59	4.6
293	1.68	5.0	331	1.30	3.2			
294	1.50	4.1	332	1.43	3.8			
295	1.37	3.5	343	1.27	3.0			
296	1.36	3.5	344	1.48	4.0			
297	1.46	3.9	348	1.27	3.0			
298	1.47	4.0	422	1.32	3.3			
TC-13	1.53	4.3	TC-23	1.28	3.1			
Mean of 10: 4.04 ± 0.4 kb			Mean of 10: 3.47 ± 0.4 kb			Mean of three: 4.2 ± 0.3 kb		

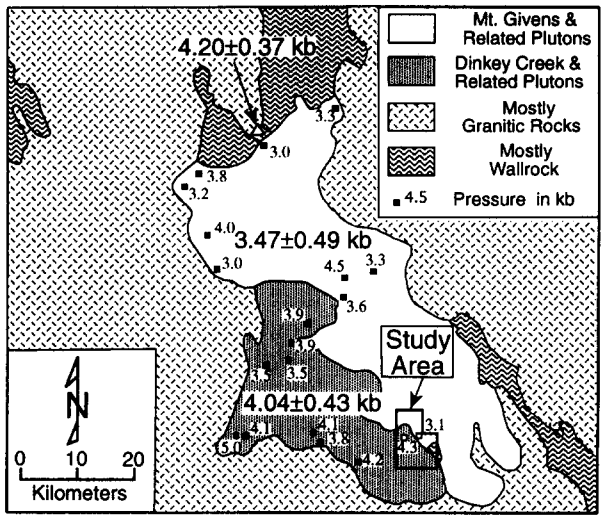

Fig. 9. Simplified geologic map showing pressure in kilobars (kb) calculated from Al^T in hornblende in the DCP (10 samples), MGP (10 samples) and the JLP (three samples, Jackass Lakes pluton). Raw data are from appendix D in Ague & Brimhall (1988, GSA Data Repository Item 8813), with the exception of two samples (open boxes) from this study; all data calculated using Schmidt's (1992) equation given in the text; see Tables 1 and 2 and captions, this study. Figures in large print on the map show mean values and their standard deviation.

appendix D) data from the same plutons which we have recalculated using Schmidt's equation, and the total pressure data are plotted in Fig. 9. We take the means of ~4 kb for the DCP and ~3.5 kb for the MGP as reasonable estimates for the confining pressures prevailing during their emplacement (Fig. 9, Tables 1 and 2; based on the composition of aplite from H_2O-saturated residual melt, however, Noyes *et al.* (1983) estimated the confining pressure during emplacement for the roughly contemporaneous Eagle Peak granodiorite as 1±0.5 kb).

Microprobe analyses of rims from igneous plagioclase from a sample of the Dinkey Creek composite pluton (TC-13, Fig. 2.) outside the shear zone were very consistent and yielded an average composition of andesine (An_{30}; Table 1), closely comparable to their recrystallized equivalents in mylonite (An_{31}) and ultramylonite (An_{34}) in the shear zone. Using the microprobe data listed in Table 1, and given the mean confining pressure indicated in Table 2, we used the equation of Blundy & Holland (1990) to estimate the temperature of shear zone movement. Sample TC-18 comes from the middle part of the shear zone (Fig. 2), and igneous hornblende therein is incompletely recrystallized. We consider the 694°C value as representing a partially re-equilibrated igneous emplacement temperature (i.e. TC-13, 710°C), and its true value is uncertain. The ultramylonite sample TC-21 (678°C, Table 1), however, is ~10 m from the contact with the MGP (with a solidus temperature of 684°C—TC-23, Fig. 2 and Table 1), and is completely recrystallized with metamorphic hornblende and biotite defining the ultramylonitic fabric (Fig. 5c). Diopsidic pyroxene has also been observed as a contact metamorphic product overprinting the ultramylonitic assemblage. We regard the 678°C estimate of TC-21 to approximate the temperature prevailing during movement in the shear zone at least at that point, with the temperature in the zone as a whole very likely lying in the 600–680°C range. To date, mineral assemblages in the wallrock suitable for thermobarometry have not been found to enable us to independently confirm these *T–P* estimates.

GEOCHRONOLOGY

Accurate dating of the deformation in the shear zone is crucial to interpreting its regional significance, especially its age relation to other shear zones to the north. To this end, we sampled and analyzed zircons and hornblende–biotite from rocks both within and immediately adjacent to the shear zone for Pb/U and $^{40}Ar/^{39}Ar$ ages, respectively.

Zircon Pb/U analysis

Zircon data for samples from the DCP and MGP located outside the study area (Fig. 1) were previously reported by Stern *et al.* (1981), but reverse discordances cast uncertainty on their age interpretation at a level that is critical for our shear zone analysis. Our new Pb/U zircon data are given in Table 3.

Two size fractions of sample 1 from the DCP (Fig. 2) yielded externally concordant ages of 102 ± 1 Ma. The data are plotted on a concordia diagram in Fig. 10. Stern *et al.* (1981) reported a 104 Ma Pb/U age for their sample, although their uncertainty could exceed ± 10 Ma considering the reverse discordance pattern in their data. We interpret our 102 ± 1 Ma age as the igneous age of the DCP in the region of the shear zone. The identical hornblende closure ages (discussed below) in the DCP and the Short Hair Creek pluton suggest these two bodies are essentially the same age.

Sample 38 of Stern *et al.* (1981), collected ~1.5 km north of the shear zone (Fig. 1), yielded a concordant Pb/U age of ~88 Ma for the MGP, and another specimen ~27 km to the north yielded a discordant Pb/U age of ~93 Ma (Fig. 1). In an attempt to further constrain the age of the MGP, we ran a multi-size fraction of zircon (sample 2) collected ~60 km northwest of sample 38 (Fig. 1). The two finer fractions are each internally concordant, but show minor external discordance, and the coarser fraction is slightly discordant. On the Fig. 10 concordia plot, this pattern is exhibited by a slight dispersion of the data points off of the most concordant fine fraction. The relatively large uncertainties in the $^{207}Pb/^{206}Pb$ ages induced by a relatively large common lead component in the sample 2 zircon (Table 3), along with the limited dispersion prohibit meaningful discordia array analysis. The pattern exhibited by the sample 2 data suggests minor inheritance of older, probably Proterozoic, zircon, that is accentuated in the coarser fractions. The dispersion pattern coupled with the uncertainties permit an igneous age of between 86 and 93 Ma,

Table 3. Zircon isotopic age data. Sample 1 is from the DCP (locality shown in Fig. 2), and sample 2 is from the MGP (locality shown in Fig. 1)

Sample	Fraction† (μm)	Amount analyzed (mg)	Concentrations (ppm)		Atomic ratios				Isotopic ages (Ma)‡		
			^{238}U	$^{206}Pb^*$	$^{206}Pb/^{204}Pb$	$^{206}Pb^*/^{238}U$	$^{207}Pb^*/^{235}U$	$^{207}Pb^*/^{206}Pb^*$	$^{206}Pb^*/^{238}U$	$^{207}Pb^*/^{235}U$	$^{207}Pb^*/^{206}Pb^*$
1	<45	1.2	1597	22.0	1043	0.01588(11)	0.1051	0.04803(13)	101.6	101.5	101 ± 7
	45–62	1.5	1416	19.6	2064	0.01602(17)	0.1061	0.04806(07)	102.5	102.4	102 ± 4
2	45–62	1.4	821	10.3	365.8	0.01457(10)	0.0963	0.04797(23)	93.3	93.4	97 ± 11
	62–80	2.0	579	7.4	847.8	0.01469(09)	0.0972	0.04803(11)	94.0	94.2	100 ± 6
	80–100	1.4	521	6.8	985.0	0.01510(09)	0.1002	0.04814(12)	96.6	96.9	105 ± 6

*Radiogenic; non-radiogenic correction based on 25 pg blank Pb (1:18.78:15.61:38.50) and initial Pb approximations: 1:18.9:15.6:38.8 (after Chen & Tilton 1991)

†Fractions separated by grain size and magnetic properties. Magnetic properties are given as non-magnetic split at 2° side/20° front slopes for 1.7 a on Franz Isodynamic Separator. Samples hand-picked to 99.9% purity prior to dissolution. Dissolution and chemical extraction techniques modified from Krogh (1973).

‡Decay constants used in age calculations: $\lambda^{238}U = 1.55125 \times 10^{-10}$, $\lambda^{235}U = 9.8485 \times 10^{-10}$ (Jaffey *et al.* 1971); $^{238}U/^{235}U$ atom = 137.88. Uncertainties in $^{206}Pb^*/^{238}U$ and $^{207}Pb^*/^{206}Pb^*$ are given as '±' in last two figures. Uncertainties calculated by quadratic sum of total derivatives of ^{238}U and $^{206}Pb^*$ concentration and $^{207}Pb^*/^{206}Pb^*$ equations with error differentials defined as: (1) isotopic ratio determinations from standard errors ($\sigma/\sqrt{n}$) of mass spectrometer runs plus uncertainties in fractionation corrections based on multiple runs of NBS 981, 982, 983, and U500 standards; (2) spike concentrations from range of deviations in multiple calibrations with normal solutions; (3) spike compositions from external precisions of multiple isotope ratio determinations; (4) uncertainty in natural $^{238}U/^{235}U$ from Chen & Wasserburg (1981); and (5) non-radiogenic Pb isotopic compositions from uncertainties in isotope ratio determinations of blank Pb and uncertainties in composition of initial Pb from estimates of regional variations based on reference given above and consideration of rock type.

which overlaps the Pb/U ages reported for the MGP by Stern *et al.* (1981). Although we interpret the age of this large pluton as $90^{+3/-4}$ Ma, it is probably close to 90 Ma based on the $^{40}Ar/^{39}Ar$ data given below.

$^{40}Ar/^{39}Ar$ analyses of shear zone and adjacent rocks

Samples for $^{40}Ar/^{39}Ar$ dating were collected along a traverse from the Short Hair Creek–DCP plutons across the shear zone into the MGP (Fig. 2). Four samples collected show a range of textures from unrecrystallized, essentially undeformed granodiorite ~0.5 km away from the shear zone to totally recrystallized, highly deformed ultramylonite in the shear zone. Analytical procedures are given in the Appendix.

Biotites from all samples have plateau dates that are mutually indistinguishable at the 2σ level, ranging from 87.46 ± 0.53 to 88.74 ± 0.37 Ma (Fig. 11). The uniformity of biotite dates from these heterogeneous rock units suggests they are cooling ages, reflecting the most recent cooling through ~300°C (Harrison *et al.* 1985). In addition, it is likely that DCP biotites closest to the MGP were outgassed (reset) by the thermal effects of the latter.

Hornblendes from the MGP yield a weighted mean of 89.8 ± 0.2 Ma, concordant (within uncertainty) with the Pb/U zircon date reported (Fig. 10, Table 3), and nearly so with the weighted mean biotite date of 87.7 ± 0.1 Ma. These data indicate rapid cooling of the MGP, probably as a result of uplift (Renne *et al.* 1992).

Hornblende plateau dates from the DCP show progressive concordance with biotite with increasing proximity to the MGP contact. This pattern is interpreted to reflect variable diffusive $^{40}Ar^*$ loss produced during reheating by the younger intrusion, which elevated temperatures to 650–700°C at the contact (Table 1) (also Renne *et al.* in press). The least affected hornblende (TC-13) yields a plateau date (94.1 ± 0.2 Ma) identical to the hornblende K–Ar date of 94 Ma in the DCP sampled ~9 km from TC-13 and ~7.5 km from the MGP contact (Kistler *et al.* 1965; age recalculated with modern decay constants). We interpret the 94 Ma age as reflecting the original igneous hornblende cooling age, free of partial resetting effects from the MGP.

Recrystallized hornblende from the shear zone yielded a plateau date of 90.2 ± 0.2 Ma, concordant at the 2σ level with the mean hornblende cooling age (89.8 ± 0.2 Ma) for the MGP. Because the hornblende grew at ~700°C (well above its Ar closure temperature, ~500°C; Harrison 1981) as the foliation was forming (cf. Figs. 5b & c), this concordance of ages reflects the thermal signature of the MGP on the developing shear zone. The regional thermal history of the DCP indicates that heating which accompanied shear zone activity occurred after ~94 Ma, and therefore deformation is constrained to have occurred during the interval 94–90 Ma. A more detailed discussion of the thermal history and its relation to the deformation will be presented elsewhere (Renne *et al.* in press).

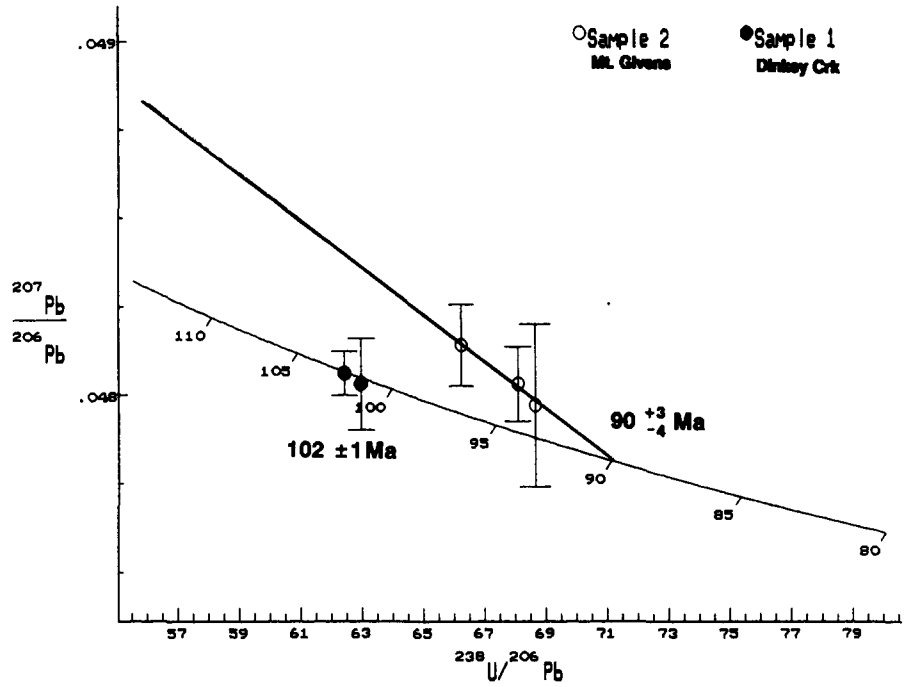

Fig. 10. Plot of samples 1 and 2 U/Pb zircon data on a $^{207}Pb/^{206}Pb$ vs $^{206}Pb/^{238}U$ concordia diagram (after Tera & Wasserburg 1972). Sample 1 data (DCP) is internally and externally concordant at 102 ± 1 Ma. Sample 2 data (MGP) is externally discordant, probably due to the minor inheritance of older zircon; the igneous age could range from 93 to 86 Ma considering the possible range of the inheritance trajectories and their lower intercepts, and is noted as $90^{+3/-4}$ Ma.

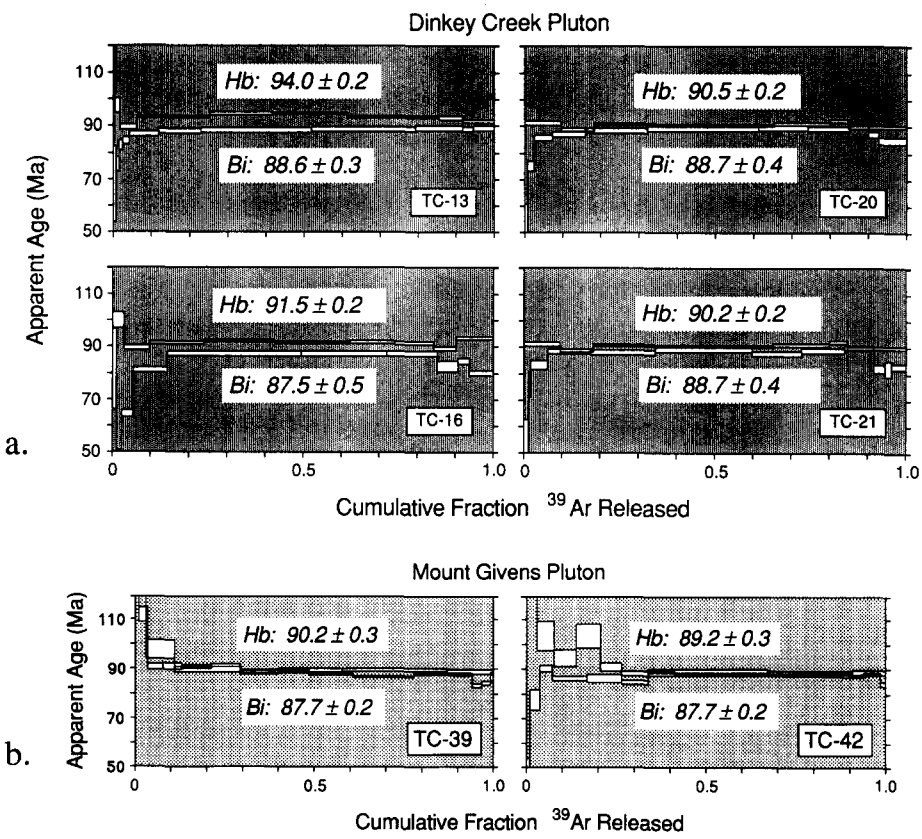

Fig. 11. (a) Apparent age spectra for hornblende–biotite pairs from samples (numbered in inset boxes) of the Short Hair Creek and Dinkey Creek granodiorites. Vertical bars represent 1σ inter-laboratory uncertainties. Plateau ages in Ma for hornblende (Hb, upper spectrum) and biotite (Bi, lower spectrum) are shown. The uncertainties on these are 1σ inter-laboratory values. (b) Apparent age spectra for hornblende–biotite pairs from samples of the MGP. Explanation is the same as for (a).

DISCUSSION

In their preliminary assessment, Bateman *et al.* (1984) considered three possibilities to explain the genesis of the shear zone at Courtright: (a) regional deformation post-dating the DCP but pre-dating the MGP; (b) protoclastic foliation generated with the late stages of emplacement of the DCP; and (c) deformation related to the forcible emplacement of the MGP. They concluded that regional deformation (a) best accounted for all their observations and fitted into a regional framework, although subsequently Bateman (1988) reconsidered (c) as equally possible.

We agree with Bateman *et al.* (1984) that (b) is unlikely because the shear zone cuts across three plutons plus their wallrock and shows kinematic west-side-down movement. In our opinion, regional deformation (a) *by itself* is also unlikely because the high temperature of deformation would require a source of high heat flow which would presumably be recorded over a larger area than the shear zone, unless it was a focused fluid-transported heat for which there is no petrologic evidence (i.e. no hydrothermal alteration products were observed). In addition, primary textures of the Short Hair Creek granodiorite ~500 m west of the shear zone show no evidence (Fig. 5a) for a wider spread high-temperature thermal zone, nor have we found evidence for the presence of fluid-related deformation within the shear zone (e.g. Tobisch *et al.* 1991a).

In our preliminary interpretation of the data (Tobisch *et al.* 1991b, c), we proposed that the shear zone resulted from shear and flattening strains imposed by the ascent and emplacement of the MGP, which was supported by structural, metamorphic and geochronological data. To have sufficient strength to impose a shear strain on the pre-existing rocks during its ascent, however, the MGP must have possessed a relatively high viscosity. Experiments by Van der Molen & Paterson (1979) indicate that *under experimental conditions*, the strength of partially (i.e. 24%) melted granite is <1 MPa at high strain rates (10^{-5} s^{-1}), which would not be sufficiently strong to induce much shear strain. Many changing factors that are likely to influence the viscosity of a large volume of ascending magma (i.e. the MGP > 15,000 km^3), however, cannot be reproduced or evaluated in the small volume (~2 cm^3) specimen available to the experimentalist. These factors might include km-scale gradients in temperature and P_{H_2O}, size, total content and contiguity of grains, their distribution in the melt (e.g. clumping of grains, etc.), thixotropic effects, and other factors (Wickham 1987, Miller *et al.* 1988).

If the Mt Givens magma was near its critical melt fraction (CMF approximately 30–40%?, Arzi 1978, Van der Molen & Paterson 1979, Wickham 1987, Miller *et al.* 1988) during the last several kilometers of its ascent and emplacement, we think that it could cause deformation by shouldering aside the wallrock to produce the $S_{2\,con}$ structures, and the evidence presented earlier supports this interpretation; it is also conceivable it could impose a small amount of shear strain, if the wallrock were sufficiently weakened by the accompanying magmatic heat. However, the *high total strain* and the high component of *shear strain* documented in the zone require other dynamic input, and we think a regional strain was involved in the shear zone development.

We are presently developing a tectonic model for the larger central Sierra Nevada (Tobisch *et al.* 1992, and in preparation), which posits that an extensional environment was active within the central Sierra Nevada magmatic arc. Recent moment tensor analysis of earthquakes has documented tensional stress regimes acting normal to modern magmatic arcs in the Pacific Basin (Apperson 1991), which presumably develop arc-parallel normal faults. The shear zone at Courtright shows many characteristics of a very steeply SW-dipping (Figs. 2 and 8a) normal fault or ductile shear zone, which displays relatively small(?) west-side-down displacement. We envision that the shear zone initiated within a weak regional extensional field as a narrow normal fault–ductile shear zone prior to the immediate proximity of the MGP (Fig. 12, Stage 1). The early (low to moderate temperature?) stages of solid-state foliation developed at this time, possibly accounting for the strong crystal-plastic deformation of relic igneous quartz found in some specimens of ultramylonite. As the MGP ascended, its heat envelope acted as a catalyst for recrystallization and deformation in the shear zone, broadening the zone and intensifying S_1 and $S_{2\,ext}$ structures (Fig. 12, Stage 2). The high-temperature mineral assemblage was developing at this time, and probably destroyed most of the lower temperature fabric formed at an early stage of shear zone movement; in addition it facilitated further ascent of the MGP and formation of $S_{2\,con}$ structures that were generated during the final stages of emplacement (Fig. 12, State 3).

It is not possible to know what component of the total strain in the shear zone was contributed by the MGP. Our present data supports the interpretation that $S_{2\,con}$ structures (e.g. Figs. 4a, b & d) represent late-emplacement deformation imposed by the MGP, with the pluton contributing to the development of the main shear zone fabric (S_1 and $S_{2\,ext}$) mostly by its heat and fluids (e.g. the migmatites in areas A and B, Fig. 2). The intense stretching lineation and mylonitic foliation observed in the wallrock (e.g. Figs. 3a and 4a) may be the combined effect of shear zone strain related to the regional strain field, downflow of wallrock during pluton emplacement such as found in wallrock screens elsewhere in the batholith (e.g. Tobisch *et al.* 1986, Saleeby *et al.* 1990), and ascent dynamics of the MGP.

CONCLUSIONS

Solid-state foliation, lineation, minor folds of the foliation and discrete shear domains have developed in the Shaver Intrusive suite, the adjacent wallrock, and an enclave-rich precursor to the MGP. This deformation was imposed by the combination of a regional extensional strain field and the ascent and emplacement of the MGP

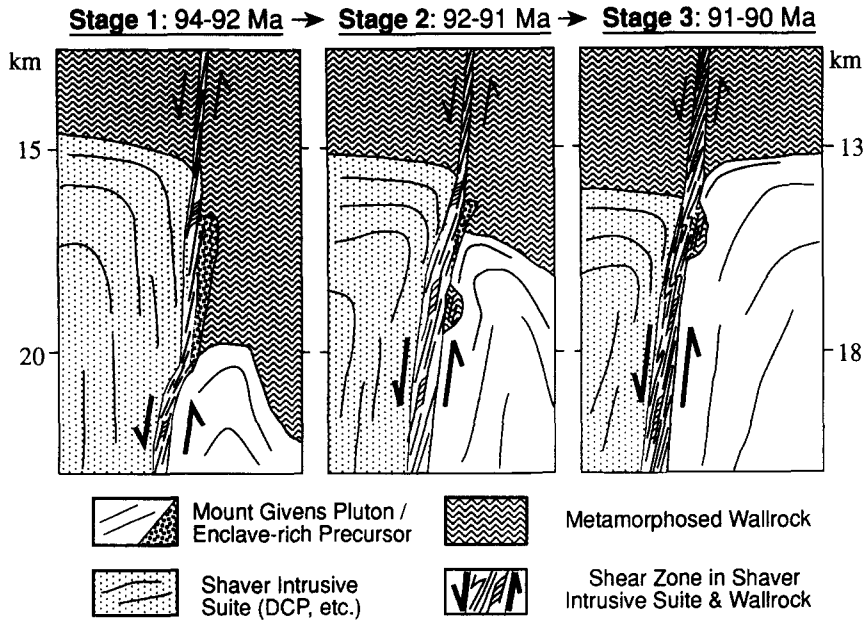

Fig. 12. Diagram illustrating the concept of a regional normal fault–ductile shear zone facilitating the buoyant rise of the MGP, further deformation on the zone being catalyzed by magmatic heat and producing the high-temperature fabrics. Some ascent- and emplacement-related strain developed in the granitoids and sedimentary wallrock as the MGP rose and overtook the enclave-rich precursor: wallrock screens may have been episodically dragged along and/or concomitantly subjected to 'return flow movement' with the Shaver Intrusive Suite. The shear zone diagrammatically shows the successive development of S_1, $S_{2\,ext}$ and $S_{2\,con}$. The specific age designation shown at the top of each panel is not well constrained but represents a reasonable scenario given our data.

between 94 and 90 Ma. Strains associated with this deformation as estimated from enclave shape show increasing intensity ($\mathcal{E}_s$) and increasing ratio of simple shear/pure shear toward the MGP contact, which suggests that the pluton used the weakest zone to ascend. The physical conditions of shear zone development at its later stages have been estimated from microprobe data for hornblende and plagioclase at $P = \sim 3.5$ kb and $T = \sim 680$°C, although conditions obviously must have changed along the shear zone as the MGP ascended to its present level. The abundance of migmatite associated with ultramylonite fabrics and melt lying parallel to S_2 axial planes in the northern half of the shear zone are not found in its southern half, and physical conditions there were probably somewhat different during shear zone development. In addition, visual estimate (using a quartz wedge) of slip systems in quartz reveals ⟨*a*⟩ slip as predominant with ⟨*c*⟩ slip a lesser component. This suggests that at least some deformation of quartz occurred at $T < 600$°C (Blumenfeld *et al.* 1986), and is a relic of early stages of regional shear, and/or the very late stages in the shear zone history after its high-temperature phase.

Lastly, it is not possible to know the original extent of the shear zone because its northern and southern extensions have been engulfed by the MGP and related plutons (e.g. Eagle Peak pluton) at late stages of their emplacement. Nevertheless, we think the Courtright shear zone represents movement in a weakly extensional environment related to regional crustal inflation which facilitated the emplacement of the MGP, and was accompanied by uplift and/or denudation (Renne *et al.* in press).

Acknowledgements—We gratefully acknowledge support from NSF grants EAR 9002672 (O. T. Tobisch), EAR 9105692 (J. B. Saleeby) and from the Geochronological Center, Institute of Human Origins (P. R. Renne). Paula Cornejo was most helpful in advising us on microprobe sample preparation and data reduction, and her expertise and those of the Stanford University staff at running the microprobe are greatly appreciated. We thank Paul C. Bateman for stimulating discussions and comments on the manuscript, Alan Thompson for counsel on interpreting the hornblende microprobe data, and an anonymous reviewer's pertinent comments, all of which helped clarify our ideas.

REFERENCES

Ague, J. J. & Brimhall, G. H. 1988. Regional variations in bulk chemistry, mineralogy, and the compositions of mafic and accessory minerals in the batholiths of California. *Bull. geol. Soc. Am.* **100**, 891–911.

Apperson, K. D. 1991. Stress fields of the overriding plate at convergent margins and beneath active volcanic arcs. *Science* **254**, 670–678.

Arzi, A. A. 1978. Critical phenomena in the rheology of partially melted rocks. *Tectonophysics* **44**, 173–184.

Bateman, P. C. 1965. Geologic map of the Blackcap Mountain quadrangle, Fresno County, California. *U.S. geol. Surv. Map* **GQ-428.**

Bateman, P. C. 1988. Constitution and genesis of the central part of the Sierra Nevada batholith, California. *U.S. geol. Surv. Open-file Rep.* **88–382.**

Bateman, P. C., Busacca, A. J. & Sawka, W. N. 1983. Cretaceous deformation in the western foothills of the Sierra Nevada. *Bull. geol. Soc. Am.* **94**, 30–42.

Bateman, P. C., Kistler, R. W. & DeGraff, J. V. 1984. Courtright intrusive zone, Sierra National Forest, Fresno County, California: a field guide. *California Geol.* May issue, 91–98.

Bateman, P. C., Lockwood, J. P. & Lydon, P. A. 1971. Geologic map of the Kaiser Peak quadrangle, central Sierra Nevada, California. *U.S. geol. Surv. Map* **GQ-894.**

Bateman, P. C. & Nokleberg, W.J. 1978. Solidification of the Mount Givens granodiorite, Sierra Nevada, California. *J. Geol.* **86**, 563–579.

Bateman, P. C. & Wones, D. R. 1972. Geologic map of the Huntington Lake quadrangle, central Sierra Nevada, California. *U.S. geol. Surv. Map* **GQ-987.**

Blumenfeld, P., Mainprice, D. & Bouchez, J. L. 1986. *C*-slip in quartz from subsolidus deformed granite. *Tectonophysics* **127**, 95–115.

Blundy, J. D. & Holland, T. J. B. 1990. Calcic amphibole equilibria and a new amphibole-plagioclase geothermometer. *Contr. Miner. Petrol.* **104**, 208–224.

Blundy, J. D. & Holland, T. J. B. 1992. Calcic amphibole equilibria and a new amphibole–plagioclase geothermometer—Reply to the comments of Hammarstrom & Zen and Rutherford & Johnson. *Contr. Miner. Petrol.* **111**, 269–272.

Busby-Spera, C. J. & Saleeby, J. B. 1990. Intra-arc strike-slip fault exposed at batholithic levels in the southern Sierra Nevada, California. *Geology* **18**, 255–259.

Cebula, G. T., Kunk, M., Mehnert, H. H., Naeser, C. W., Obradovich, J. D. & Sutter, J. F. 1986. The Fish Canyon Tuff, a potential standard for the ^{40}Ar–^{39}Ar and Fission-track methods. *Terra Cognita* **6**, 139–140.

Chen, J. H. & Moore, J. G. 1982. Uranium–lead isotopic ages from the Sierra Nevada batholith, California. *J. geophys. Res.* **87**, 4761–4784.

Chen, J. H. & Tilton, G. R. 1991. Applications of lead and strontium isotopic relationships to the petrogenesis of granitoid rocks, central Sierra Nevada batholith, California. *Bull. geol. Soc. Am.* **103**, 439–447.

Chen, J. H. & Wasserburg, G. J. 1981. Isotopic determination of uranium in picomole and subpicomole quantities. *Analyt. Chem.* **53**, 2060–2067.

Courrioux, G. 1987. Oblique diapirism: the Criffel granodiorite/granite zoned pluton (southwest Scotland). *J. Struct. Geol.* **9**, 313–330.

Coward, M. P. & Kim, J. H. 1981. Strain within thrust sheets. In: *Thrust and Nappe Tectonics* (edited by McClay, K. R. & Price, N. J.). *Spec. Publs geol. Soc. Lond.* **9**, 275–292.

Deino, A. L., Tauxe, L., Monaghan, M. & Drake, R. 1990. ^{40}Ar–^{39}Ar age calibration of the litho- and paleomagnetic stratigraphies of the Ngorora Formation, Kenya. *J. Geol.* **98**, 567–587.

Escorza, C. M. 1978. Estructura y deformacion de los enclaves microgranulares negros (gabarros) del Alto de los Leones, Guadarrama. *Bol. R. Soc. Española Hist. Nat. (Geol.)* **76**, 57–87.

Gazis, C. & Saleeby, J. 1991. Southward continuation of the Proto-Kern Canyon fault zone (PFK) to the upper Caliente Creek area, southern Sierra Nevada. *Geol. Soc. Am. Abs. w. Prog.* **23**, 28.

Hammarstrom, J. M. & Zen, E-an 1986. Aluminum in hornblende: an empirical igneous geobarometer. *Am. Miner.* **71**, 1297–1313.

Hammarstrom, J. M. & Zen, E-an 1992. Discussion of Blundy and Holland's (1990) "Calcic amphibole equilibria and a new amphibole–plagioclase geothermometer". *Contr. Miner. Petrol.* **111**, 264–266.

Harrison, T. M. 1981. Diffusion of ^{40}Ar in hornblende. *Contr. Miner. Petrol.* **78**, 324–331.

Harrison, T. M., Duncan, I. & McDougall, I. 1985. Diffusion of ^{40}Ar in biotite: Temperature, pressure and composition effects. *Geochim. cosmochim. Acta* **49**, 2461–2468.

Holder, M. T. 1979. An emplacement mechanism for post tectonic granites and its implications for their geochemical features. In: *Origin of Granite Batholiths—Geochemical Criteria* (edited by Atherton, M. P. & Tamey, J.). Shiva, Orpington, Kent, 116–128.

Hollister, L. S., Grissom, G. C., Peters, E. K., Stowell, H. H. & Sisson, V. B. 1987. Confirmation of the empirical correlation of Al in hornblende with pressure of solidification of calc-alkaline plutons. *Am. Miner.* **72**, 231–239.

Hutton, D. H. W. 1982. A method for the determination of the initial shapes of deformed xenoliths in granitoids. *Tectonophysics* **85**, T45–T50.

Jaffey, A. H., Flynn, K. F., Glendenin, L. E., Bentley, W. C., & Essling, A. M. 1971. Precision measurement of the half-lives and specific activities of ^{235}U and ^{238}U. *Phys. Rev.* **C4**, 1889–1906.

Johnson, M. C. & Rutherford, M. J. 1989. Experimentally determined conditions in the Fish Canyon Tuff, Colorado, magma chamber. *J. Petrol.* **30**, 711–737.

Kistler, R. W. & Bateman, P. C. 1966. Stratigraphy and structure of the Dinkey Creek roof pendant in the central Sierra Nevada, California. *Prof. Pap. U.S. geol. Surv.* **524-B.**

Kistler, R. W., Bateman, P.C. & Brannock, W. W. 1965. Isotopic ages of minerals from granitic rocks of the central Sierra Nevada and Inyo Mountains, California. *Bull. geol. Soc. Am.* **76**, 155–164.

Kligfield, R., Carmignani, L. & Owens, W. H. 1981. Strain analysis of a Northern Apennine shear zone using deformed marble breccias. *J. Struct. Geol.* **3**, 421–436.

Krogh, T.E. 1973. A low contamination method for hydrothermal decomposition of zircon and extraction of U and Pb for isotopic age determinations. *Geochim. cosmochim. Acta* **37**, 485–494.

Lahren, M. M. & Schweickert, R. A. 1989. Proterozoic and Lower Cambrian miogeoclinal rocks of the Snow Lake pendant, Yosemite–Emigrant Wilderness, Sierra Nevada, California: Evidence for major Early Cretaceous dextral translation. *Geology* **17**, 156–160.

Lockwood, J. P. & Bateman, P. C. 1976. Geologic map of the Shaver Lake quadrangle, central Sierra Nevada, California. *U.S. geol. Surv. Map* **GQ-1271**.

Lode, W. 1926. Versuche über den Einfluss der mittleren Hauptspannung auf das fliessen des Metalle Eisen, Kupfer, und Nickel. *Z. Phys.* **36**, 913–939.

McNulty, B. A. 1991. Development of mylonite and pseudotachylite(?) in the Bench Canyon shear zone, central Sierra Nevada, California. *Geol. Soc. Am. Abs. w. Prog.* **23**, A176–A177.

Merritt, N. J. 1985. The Dinkey Creek pendant, central Sierra Nevada: A pre-Nevadan(?) deep crustal shear zone. *Geol. Soc. Am. Abs. w. Prog.* **17**, 369.

Miller, C. F., Watson, E. B. & Harrison, T. M. 1988. Perspectives on the source, segregation and transport of granitoid magmas. *Trans. Roy. Soc. Edin., Earth Sci.* **79**, 135–156.

Nadai, A. 1963. *Theory of Flow and Fracture of Solids* (2nd edn). McGraw-Hill, New York.

Noyes, H. J., Wones, D. R. & Frey, F. A. 1983. A tale of two plutons: petrographic and mineralogic constraints on the petrogenesis of the Red Lake and Eagle Peak plutons, central Sierra Nevada, California. *J. Geol.* **91**, 353–379.

Passchier, C. W. & Simpson, C. 1986. Porphyroclast systems as kinematic indicators. *J. Struct. Geol.* **8**, 831–843.

Paterson, S. R., Vernon, R. H. & Tobisch, O. T. 1989. A review of criteria for the identification of magmatic and tectonic foliations in granitoids. *J. Struct. Geol.* **11**, 349–363.

Peck, D. L. 1980. Geologic map of the Merced Peak quadrangle, central Sierra Nevada, California. *U.S. geol. Surv. Map* **GQ-1531**.

Poli, S. & Schmidt, M. W. 1992. A comment on "Calcic amphibole equilibria and a new amphibole–plagioclase geothermometer" by J. D. Blundy & T. J. B. Holland. *Contr. Miner. Petrol.* **111**, 273–282.

Ramsay, J. G. 1967. *Folding and Fracturing of Rocks*. McGraw Hill, New York.

Ramsay, J. G. 1975. The structure of the Chindamora Batholith. *19th Ann. Rep. Res. Inst. African Geol., Univ. Leeds* **81**.

Ramsay, J. G. 1989. Emplacement kinematics of a granite diapir: the Chindamora batholith, Zimbabwe. *J. Struct. Geol.* **11**, 191–209.

Ramsay, J. G. & Huber, M. I. 1983. *The Techniques of Modern Structural Geology, Volume* 1: *Strain Analysis*. Academic Press, London.

Renne, P. R., Tobisch, O. T. & Saleeby, J. B. In press. Thermochronologic record of pluton emplacement, deformation and exhumation at Courtright Shear Zone, central Sierra Nevada. *Geology*.

Rutherford, M. J. & Johnson, M. C. 1992. Comment on Blundy and Holland's (1990) Calcic amphibole equilibria and a new amphibole–plagioclase geothermometer. *Contr. Miner. Petrol.* **111**, 266–268.

Saleeby, J. 1992. Structure of the northern segment of the proto-Kern Canyon fault zone (PKCFZ), southern Sierra Nevada, California. *Geol. Soc. Am. Abs. w. Prog.* **24**.

Saleeby, J. B., Kistler, R. W., Longiaru, S., Moore, J. G. & Nokleberg, W. J. 1990. Middle Cretaceous silicic metavolcanic rocks in the Kings Canyon area, central Sierra Nevada, California. In: *The Nature and Origin of Cordilleran Magmatism* (edited by Anderson, J. L.). *Mem. geol. Soc. Am.* **174**, 251–270.

Schmidt, M. W. 1992. Amphibole composition in tonalite as a function of pressure: an experimental calibration of the Al-in-hornblende barometer. *Contr. Miner. Petrol.* **110**, 304–310.

Stern, T. W., Bateman, P. C., Morgan, B. A., Newell, M. F. & Peck, D. L. 1981. Isotopic U-Pb ages of zircon from the granitoids of the central Sierra Nevada, California. *Prof. Pap. U.S. geol. Surv.* **1185**.

Tera, F. & Wasserburg, G. J. 1972. U/Pb systematics in lunar basalts. *Earth Planet Sci. Lett.* **17**, 65–78.

Tikoff, B. & Teyssier, C. 1991. Dextral shearing in the east-central Sierra Nevada magmatic arc: implications for Late Cretaceous tectonics and passive emplacement of granite. *Geol. Soc. Am. Abs. w. Prog.* **23**, A176.

Tobisch, O. T., Barton, M. D., Vernon, R. H. & Paterson S. R. 1991a. Fluid-enhanced deformation: transformation of granitoids to banded mylonites, western Sierra Nevada, California, and southeastern Australia. *J. Struct. Geol.* **13**, 1137–1156.

Tobisch, O. T., Paterson, S. R. & Tong, W. 1990. Nature of ductile shear zones in granitic rocks of the central Sierra Nevada, California: implications for batholith emplacement models. *Geol. Soc. Am. Abs. w. Prog.* **22**, 89.

Tobisch, O. T., Renne, P. R. & Saleeby, J. B. 1991b, A case for pluton ascent- and emplacement deformation: the Courtright ductile shear

zone, central Sierra Nevada batholith, California. *Mitt. Geol. Inst. ETH Zürich, N.F.* **239b**, 73–74.
Tobisch, O. T., Renne, P. R. & Saleeby, J. B. 1991c. Pluton emplacement dynamics and shear zone kinematics at Courtright, central Sierra Nevada, California: Evidence from $^{40}A/^{39}A$ and Pb/U thermochronology and hornblende barometry. *Geol. Soc. Am. Abs. w. Prog.* **23**, A176.
Tobisch, O. T., Saleeby, J. B. & Fiske, R. S. 1986. Structural history of continental volcanic arc rocks, eastern Sierra Nevada, California: a case for extensional tectonics. *Tectonics* **5**, 65–94.
Tobisch, O. T., Saleeby, J. B., Renne, P. R., McNulty, B. & Tong, W. 1992. Dynamics of emplacement of a large volume magmatic arc (LVMA), central Sierra Nevada (CSN), California. *Geol. Soc. Am. Abs. w. Prog.* **24**, 86.
Tong, W. 1991. Heterogeneous ductile shearing in the central Sierra Nevada batholith: a retrograde deformation. *Geol. Soc. Am. Abs. w. Prog.* **23**, A176.
Turner, F. J. 1981. *Metamorphic Petrology: Mineralogical, Field and Tectonic Aspects*. McGraw-Hill, New York.
Van der Molen, I. & Paterson, M. A. 1979. Experimental deformation of partially-melted granite. *Contr. Miner. Petrol.* **70**, 299–318.
Vernon, R. H. 1991. Questions about myrmekite in deformed rocks. *J. Struct. Geol.* **13**, 979–986.
Vernon, R. H., Etheridge, M. A. & Wall, V. J. 1988. Shape and microstructure of microgranitoid enclaves: indicators of magma mingling and flow. *Lithos* **22**, 1–11.
Vyhnal, C. R., McSween, H. Y., Jr., & Speer, J. A. 1991. Hornblende chemistry in southern Appalachian granitoids: implications for aluminium–hornblende thermobarometry and magmatic epidote stability. *Am. Miner.* **76**, 176–188.
Wickham, S. M. 1987. The segregation and emplacement of granitic magmas. *J. geol. Soc. Lond.* **144**, 281–297.

APPENDIX

Analytical procedures for $^{40}Ar/^{39}Ar$

Hornblende and biotite were separated from the 20–60 mesh fraction of each sample, then washed with distilled water in an ultrasonic cleaner. Hornblende was further rinsed in 5% HF for 3 min. Several grains from each of the 12 mineral separates were then placed in pits of Al disks and irradiated for approximately 28 h in the Omega West Reactor at Los Alamos National Laboratory, along with the interlaboratory standard Fish Canyon sanidine (Cebula *et al.* 1986) for which a reference age of 27.84 Ma was used. The Dinkey Creek samples (TC-13 – TC-21) and the Mount Givens samples (TC-39 and TC-42) were irradiated in different batches, reflected by the different values of J (a measure of the fast neutron fluence) for the different samples. All samples and standards in a given batch were within 2 mm vertically of one another during irradiation.

Single grains of each sample were incrementally degassed for 30 s in 8–12 steps, up to fusion, with an Ar ion laser under a defocused beam. Gas so liberated was purified with two SAES-172 getters operated at 3 A and a cryo-cooled condensation trap operated at −50°C. After purification for 3–5 min, relative abundances of the Ar isotopes were measured using a MAP-215C noble gas mass spectrometer. Laser power output, pneumatically actuated valve operation and mass spectroscopy were performed in fully automated mode according to computer-programmed specifications (Deino *et al.* 1990). Ion beams were measured on a Balzers electron multiplier operated for most samples at 1.4 kV, except hornblendes from TC-39 and TC-42, which were run at 1.6 kV. Data corrected for mass discrimination, interfering nuclear reactions and atmospheric contamination were used to calculate apparent ages, summarized in Table A1 and Fig. 11. All samples yielded apparent age plateaux of varying quality, and plateau dates were calculated as the inverse variance weighted mean of dates from consecutive steps within 2σ of the weighted mean.

Table A1. Summary of $^{40}A/^{39}A$ data. All data were collected by a single crystal laser probe; details of the analytical procedure are given in the Appendix

Laser	$^{40}Ar^*/^{39}Ar$	$\%^{40}Ar^*$	^{39}Ar	Age	±1 SD
TC-13 BIO Dinkey Creek pluton					
A-O.2†	2.1020	1.4	0.0155	72.02	39.82
B-0.4	1.9831	3.3	0.1536	68.02	14.45
C-0.6	2.2111	18.6	0.1335	75.68	2.80
D-0.8	2.4241	27.8	0.1888	82.81	1.98
E-1.0	2.4736	45.6	0.3581	84.46	1.28
F-1.4	2.5471	66.9	1.4759	86.91	0.97
G-1.8	2.5890	84.9	2.1801	88.30	0.93
H-2.4	2.6001	95.4	5.6451	88.67	0.92
I-3.0	2.6082	97.5	5.2967	88.94	0.92
J-3.6	2.6142	97.5	2.4224	89.14	0.94
K-4.0	2.6096	96.6	0.5581	88.99	0.94
L-6.0*	2.6171	93.9	1.0740	89.24	0.93
Plateau = 88.62 ± 0.35 Ma (steps F–L)					
TC-16 BIO Dinkey Creek pluton					
A-0.2†	−2.1070	−5.3	0.0045	−75.20	22.78
B-0.4	2.3867	12.2	0.0764	81.56	15.29
C-0.6	1.4038	16.2	0.1377	48.42	2.21
D-0.8	1.8802	34.6	0.2533	64.56	1.31
E-1.0	2.3721	67.1	0.7351	81.07	0.93
F-1.4	2.5639	91.2	2.9488	87.47	0.91
G-1.8	2.5639	91.9	1.8916	87.47	0.91
H-2.4	2.5627	85.1	1.1078	87.43	0.93
I-3.0	2.4187	74.4	0.4621	82.63	2.18
J-3.6	2.4816	75.2	0.2521	84.73	1.07
K-6.0*	2.3454	69.2	0.5204	80.18	0.92
Plateau = 87.46 ± 0.53 Ma (steps F–H)					
TC-20 BIO Dinkey Creek pluton					
A-0.4†	1.4597	3.7	0.0385	50.32	10.43
B-0.6	2.1881	36.9	0.0919	74.91	1.86
C-0.8	2.5102	63.3	0.2308	85.68	1.08
D-1.0	2.5533	84.7	0.4435	87.12	0.94
E-1.2	2.5915	93.0	0.8190	88.39	0.92
F-1.4	2.6217	95.9	1.4574	89.39	0.93
G-1.8	2.6263	98.1	0.6627	89.54	0.93
H-2.4	2.6201	86.5	0.5501	89.34	0.96
I-3.0	2.6416	83.9	0.2390	90.05	1.04
J-3.6	2.5561	91.3	0.1356	87.21	1.10
K-6.0*	2.4823	48.4	0.3666	84.75	1.24
Plateau = 88.74 ± 0.37 Ma (steps D–J)					
TC-21 BIO Dinkey Creek pluton					
A-0.3†	1.4482	3.1	0.0303	49.93	12.77
B-0.4	2.2194	31.4	0.0183	75.96	4.66
C-0.6	2.4408	46.3	0.1182	83.36	1.51
D-0.8	2.5915	85.5	0.2920	88.39	0.98
E-1.0	2.5820	92.9	0.4538	88.07	0.93
F-1.2	2.6122	96.6	0.6665	89.08	0.93
G-1.4	2.5771	96.1	0.3434	87.91	0.93
H-1.8	2.6091	96.4	0.2947	88.97	0.95
I-2.4	2.6357	94.9	0.1963	89.86	0.99
J-3.0	2.3992	86.3	0.0806	81.98	1.55
K-3.6	2.3981	85.5	0.0481	81.94	2.90
L-6.0*	2.4264	88.0	0.0960	82.88	1.16
Plateau = 88.69 ± 0.39 Ma (steps D–I)					
TC-39 BIO Mt Givens pluton					
A-0.3	33.8321	6.7	0.4955	1036.82	72.86
B-0.4	2.4309	13.8	1.2594	97.96	3.74
C-0.5	2.2198	39.5	2.9275	89.66	1.06
D-0.6	2.1970	60.1	3.0408	88.76	0.48
E-0.7	2.1762	76.9	1.9697	87.94	0.42
F-0.9	2.1494	78.2	2.7119	86.89	0.30
G-1.2	2.1737	71.0	1.6836	87.84	0.37
H-1.5	2.1753	58.7	0.9051	87.91	0.57
I-1.8	2.0550	56.8	0.4461	83.16	0.69
J-2.5	2.0823	54.5	0.3734	84.24	0.80
K-3.0*	2.1528	54.5	0.1248	87.02	1.62
Plateau = 87.72 ± 0.18 Ma (steps E–J)					

Table A1. *Continued*

Laser	$^{40}Ar^*/^{39}Ar$	$\%^{40}Ar^*$	^{39}Ar	Age	±1 SD
TC-42 BIO Mt Givens pluton					
A-0.3	44.6699	7.9	0.5330	1273.26	71.33
B-0.4	2.5734	9.8	0.8709	103.54	5.92
C-0.5	2.3403	14.9	1.1365	94.40	3.32
D-0.6	2.5721	11.5	1.1962	103.49	4.83
E-0.7	2.2594	30.2	1.0737	91.22	1.70
F-0.9	2.1913	46.3	2.6627	88.54	0.85
G-1.2	2.1744	78.1	5.4790	87.87	0.28
H-1.5	2.1610	77.6	2.9777	87.34	0.30
I-1.8	2.1605	66.7	1.0728	87.32	0.48
J-2.5	2.1821	63.2	0.8206	88.18	0.50
K-3.0*	2.0770	55.4	0.2572	84.03	0.99
Plateau = 87.71 ± 0.18 Ma (steps C–H)					
TC-13 HBL Dinkey Creek pluton					
A-0.5	5.1148	17.0	0.0210	170.48	9.65
B-0.9	2.8695	67.4	0.0500	97.62	2.70
C-1.2	2.6265	81.1	0.1690	89.55	0.83
D-1.4	2.7468	97.9	0.7360	93.55	0.37
E-1.6	2.7842	98.3	0.6360	94.79	0.46
F-1.8	2.7828	99.7	0.7520	94.74	0.33
G-2.0	2.7422	97.3	0.9390	93.40	0.39
H-2.5	2.7328	98.0	0.2450	93.08	0.71
I-4.0*	2.6937	97.3	0.3150	91.78	0.60
Plateau = 94.05 ± 0.18 Ma (steps D–H)					
TC-16 HBL Dinkey Creek pluton					
A-0.5	2.9423	24.4	0.1190	100.03	2.93
B-0.9	2.6258	82.4	0.2680	89.53	0.83
C-1.2	2.6823	92.6	0.5680	91.41	0.41
D-1.4	2.7103	97.3	0.7340	92.34	0.36
E-1.6	2.6923	98.0	0.7880	91.74	0.37
F-1.8	2.6948	97.5	0.4630	91.82	0.49
G-2.0	2.6794	97.8	0.4090	91.31	0.56
H-2.5	2.6850	92.5	0.2410	89.47	0.66
I-4.0*	2.7379	99.2	0.3850	93.25	0.47
Plateau = 91.53 ± 0.18 Ma (steps B–H)					
TC-20 HBL Dinkey Creek pluton					
A-0.5	2.6764	53.8	0.3900	91.21	0.82
B-0.9	2.6097	85.8	0.3630	88.99	0.56
C-1.2	2.6689	97.3	0.6700	90.96	0.46
D-1.4	2.6533	98.9	0.6890	90.44	0.38
E-1.6	2.6564	97.3	0.5740	90.55	0.40
F-1.8	2.6711	98.2	0.6090	91.04	0.46
G-2.0	2.7068	97.8	0.1950	92.22	0.69
H-4.0*	2.6394	96.8	0.6340	89.98	0.42
Plateau = 90.54 ± 0.17 Ma (steps A–H)					
TC-21 HBL Dinkey Creek pluton					
A-0.5	4.2639	19.9	0.0520	143.21	6.44
B-0.9	2.7735	75.4	0.0540	94.43	2.10
C-1.2	2.5575	81.0	0.2140	87.25	0.99
D-1.4	2.6428	95.8	0.4830	90.09	0.45
E-1.6	2.6723	97.1	0.8940	91.07	0.41
F-1.8	2.6406	97.2	0.9090	90.02	0.40
G-2.0	2.6396	98.7	0.5680	89.98	0.42
H-2.5	2.6171	92.1	0.2700	89.24	0.74
I-4.0*	2.4291	85.2	0.0640	82.97	1.82
Plateau = 90.22 ± 0.20 Ma (steps D–H)					
TC-39 HBL Mt Givens pluton					
A-0.5	9.7399	29.9	0.8588	364.03	9.33
B-0.9	2.7885	32.7	2.4871	111.93	2.80
C-1.2	2.2522	57.4	4.0418	90.94	1.07
D-1.4	2.2564	74.9	5.2188	91.10	1.42
E-1.6	2.2547	83.4	7.7728	91.04	0.72
F-1.8	2.2664	83.4	7.7990	91.50	0.68
G-2.0	2.2028	71.6	10.5384	88.99	0.87
H-2.4	2.2134	86.6	16.7414	89.41	0.58
I-2.8	2.2219	92.3	28.0319	89.74	0.52
J-3.5*	2.1996	92.0	12.5754	88.87	0.95
Plateau = 90.09 ± 0.26 Ma (steps C–J)					
TC-42 HBL Mt Givens pluton					
A-0.5	0.6726	1.2	0.7727	27.64	26.16
B-0.9	1.9091	18.1	2.4165	77.38	4.35
C-1.2	2.2380	47.8	3.2103	90.38	1.36
D-1.4	2.1369	59.9	8.4245	86.39	1.00
E-1.6	2.1372	66.6	8.1438	86.40	1.67
F-1.8	2.0960	70.3	6.6679	84.78	0.81
G-2.0	2.2150	81.7	9.1119	89.47	0.71
H-2.4	2.2134	88.7	19.7210	89.41	0.64
I-2.8	2.2031	88.0	20.4144	89.00	0.56
J-3.5*	2.2021	80.6	8.1533	88.97	0.92
Plateau = 89.21 ± 0.34 Ma (steps G–J)					

Notes.

Dinkey Creek pluton (irradiation 45 B): $J = 0.01938 \pm 0.00002$.

Mt Givens pluton (irradiation 51 B): $J = 0.02296 \pm 0.00002$.

Laser is laser power output in W for indicated step; * indicates fusion; † indicates 50% neutral density filter used for all steps.

$\%\ ^{40}Ar^*$ is percent of ^{40}Ar that is radiogenic.

^{39}Ar is relative ion beam signal in nA.